The *Salmonella* transmembrane effector SteD hijacks AP1-mediated vesicular trafficking for delivery to antigen-loading MHCII compartments

Camilla Godlee[a*], Ondrej Cerny[a], Mei Liu[a], Samkeliso Blundell[a], Alanna E. Gallagher[a], Meriam Shahin[a] and David W. Holden[a*,]

[a]MRC Centre for Molecular Bacteriology and Infection, Imperial College London, Armstrong Road, London SW7 2AZ, UK.

*For correspondence: c.godlee@imperial.ac.uk, d.holden@imperial.ac.uk

Abstract

SteD is a transmembrane effector of the *Salmonella* SPI-2 type III secretion system that inhibits T cell activation by reducing the amounts of at least three proteins – major histocompatibility complex II (MHCII), CD86 and CD97 – from the surface of antigen-presenting cells. SteD specifically localises at the *trans*-Golgi network (TGN) and MHCII compartments; however, the targeting, membrane integration and trafficking of SteD are not understood. Using systematic mutagenesis, we identify distinct regions of SteD that are required for these processes. We show that SteD integrates into membranes of the ER/Golgi through a two-step mechanism of membrane recruitment from the cytoplasm followed by integration. SteD then migrates to and accumulates within the TGN. From here it hijacks the host adaptor protein (AP)1-mediated trafficking pathway from the TGN to MHCII compartments. AP1 binding and post-TGN trafficking require a short sequence in the N-terminal cytoplasmic tail of SteD that resembles the AP1-interacting dileucine sorting signal, but in inverted orientation, suggesting convergent evolution.

Introduction

The virulence of many bacterial pathogens relies on the delivery of effector proteins into host cells through secretion systems such as the type three secretion system (T3SS). These effectors manipulate immune responses and promote bacterial replication. Many effectors require a specific host cellular localisation for their function (1,2). A subset of bacterial effectors from diverse pathogens, localise by integrating into specific membranes of host cells. These include *Salmonella* SteD, SseF and SseG, *E. coli* Tir and *Chlamydia* Incs. These transmembrane effectors are often crucial to pathogenesis; however, their targeting, membrane integration and trafficking are poorly understood. It has been proposed that they could integrate into host membranes by either 1 – lateral transfer during translocation through the T3SS pore or 2 – direct integration following translocation into the cytoplasm (3).

Following uptake into a host cell, *Salmonella* resides within a membrane-bound compartment known as the *Salmonella*-containing vacuole (SCV), from which it delivers effectors of the *Salmonella* pathogenicity Island (SPI)-2 T3SS through the vacuolar membrane. One of these, SteD, reduces mature antigen-loaded major histocompatibility complex (mMHCII) and CD86 from the surface of infected antigen-presenting cells, resulting in a reduction in T cell activation (4). It also reduces CD97 cell surface levels, which destablises immunological synapses formed between dendritic cells and T cells (5). It thus has an inhibitory effect on the adaptive immune response to *Salmonella*. mMHCII and CD97 interact with SteD and are ubiquitinated by the NEDD4 family HECT E3 ubiquitin ligase WWP2, generating predominantly K63 linkages and resulting in their lysosomal degradation (5,6). SteD is also ubiquitinated by WWP2 in a way that augments its activity yet results in its lysosomal degradation (6). The mechanism underlying this activity involves an intramembrane interaction between SteD and the transmembrane protein TMEM127, which acts as an adaptor for WWP2 (6).

SteD is 111 amino acids in length, has two transmembrane domains and integrates into host cell membranes such that both the N and C termini are exposed to the cytoplasm, separated by a luminal loop. Interaction with the *Salmonella* chaperone SrcA is required for SteD solubility in the *Salmonella*

48 cytoplasm and efficient translocation (7). Following bacterial translocation or exogenous expression in
49 host cells, the majority of SteD is at the *trans*-Golgi network (TGN) (4). It also localises to endosomal
50 compartments including MHCII compartments, where mMHCII and CD97 are also found (4,5).

51 Despite some understanding of the protein-protein interactions required for SteD function, it remains
52 unclear how SteD integrates into membranes, what is required for its localisation, and whether its
53 localisation at the TGN is important for function. Through mutagenesis, we have found three different
54 regions of SteD that are required for its localization, integration, and vesicular trafficking. Our results
55 suggest that following translocation, a cytoplasmic intermediate of SteD is recruited to the ER or Golgi,
56 where it undergoes membrane integration before transport to the TGN. Through interaction with the
57 TGN-associated adaptor protein (AP)1 complex SteD then co-opts a post-TGN vesicular trafficking
58 pathway to MHCII compartments, where it carries out its function.

RESULTS

Two regions of SteD are required for membrane integration

Ectopic expression of GFP-SteD in antigen-presenting cells recapitulates the bacterially translocated protein with respect to subcellular localisation, membrane integration and reduction of mMHCII cell surface levels (4). This shows that these processes do not require any other *Salmonella* factor and that SteD function is not affected by the GFP tag. Therefore, we investigated the requirements for membrane integration and localisation of SteD using this system. In previous work from our group, alanine scanning mutagenesis of sequential blocks of 5-7 amino acids resulted in 20 different mutants (Fig S1A), 18 of which localised correctly at the TGN (4). The other two mutants ($SteD_{ala9}$ and $SteD_{ala13}$) were not detectable (4). In $SteD_{ala9}$, the substituted residues (LMCLG) are in the N-terminal transmembrane domain (Fig 1A). In $SteD_{ala13}$, the substituted residues (SVSSG) are in the luminal loop (Fig 1A). In the presence of MG132 (an inhibitor of proteasome degradation), both mutants were detected by immunoblot (Fig 1B), indicating that mutation of either region results in protein degradation.

Next, we analysed whether these regions are important for SteD function by measuring cell surface levels of mMHCII by flow cytometry after expression of both mutants by transfection into Mel Juso cells in the presence of MG132. As expected, wild-type (wt) GFP-SteD decreased surface levels of mMHCII compared to untransfected cells (Fig 1C and Fig S1B). For cells expressing GFP-SteD the presence of MG132 reduced but did not prevent the decrease in surface mMHCII (Fig S1C). However, in cells containing similar levels of either GFP-$SteD_{ala9}$, GFP-$SteD_{ala13}$ or GFP alone, there was no significant reduction in mMHCII surface levels (Fig 1C and Fig S1B), demonstrating that the mutated regions are required for the function of SteD.

To test whether GFP-$SteD_{ala9}$ or GFP-$SteD_{ala13}$ integrate into mammalian cell membranes we subjected transfected cells to biochemical fractionation. Cell lysates were pelleted by ultracentrifugation to distinguish cytoplasmic proteins (including actin) from membrane-associated and integral membrane

84 proteins, and then pellets were solubilised with either urea (to extract peripheral membrane proteins,
85 including Golgin-97) or RIPA buffer (to extract integral membrane proteins, including the DRα chain of
86 MHCII). As expected, wt GFP-SteD, along with DRα, was present in the pellet after the initial
87 centrifugation and the urea wash, but was solubilised by RIPA, confirming its integration into host
88 membranes. However, both GFP-SteD$_{ala9}$ and GFP-SteD$_{ala13}$ were resistant to solubilisation with RIPA
89 (Fig 1D). This indicates that neither mutant underwent membrane integration, but instead formed
90 insoluble aggregates. Therefore, amino acids within the mutated regions of SteD$_{ala9}$ (hereafter referred
91 to as Region 9) and SteD$_{ala13}$ (hereafter referred to as Region 13) are required for membrane integration
92 and functionality of SteD.

93 A two-step process for post-translocation membrane
94 integration

95 To determine how these mutations affected SteD localisation in the host cell, we examined GFP-SteD$_{ala9}$
96 and GFP-SteD$_{ala13}$ in the presence of MG132 by fluorescence microscopy. Whereas a large proportion
97 of wt GFP-SteD colocalised with the TGN marker TGN46, GFP-SteD$_{ala9}$ formed cytoplasmic punctate
98 structures that colocalised with ubiquitin (Fig 2A and Fig S2A). This, along with its resistance to
99 detergent extraction (Fig 1D) indicates that when proteasome activity is inhibited, GFP-SteD$_{ala9}$ forms
100 cytoplasmic aggregates that resemble aggresomes or inclusion bodies (8). In contrast, SteD$_{ala13}$
101 colocalised with TGN46, although to a lesser extent than wt GFP-SteD (Fig 2A and B). Time-lapse
102 microscopy revealed that wt GFP-SteD was present in motile vesicles, whereas GFP-SteD$_{ala13}$ remained
103 stably associated with the Golgi area (Video S1). Therefore, in the presence of MG132, SteD$_{ala13}$
104 remained in a Golgi-associated non-integrating state, which then formed insoluble aggregates after cell
105 lysis (Fig 1D). These results show that SteD localisation at the Golgi can be uncoupled from membrane
106 integration, with Region 9 mediating interaction with a membrane component, while Region 13 is
107 required for integration following Golgi association.

108 To test whether Region 13 promotes membrane integration of other transmembrane sequences, we
109 created a chimeric protein in which the transmembrane domains of SteD were replaced by those of
110 another *Salmonella* integral membrane effector – SseG, which has a similar membrane topology to
111 SteD. This construct ($SteD_{TMSseG}$, Fig 2C) therefore contained SteD Region 13 but lacked Region 9.
112 Fractionation experiments demonstrated that $SteD_{TMSseG}$ underwent membrane integration (Fig 2D),
113 and this was dependent on Region 13, as demonstrated by the lack of RIPA solubility following its
114 alanine substitution ($SteD_{TMSseGala13}$, Fig 2D). In contrast to SteD, SseG localised at membranes
115 throughout the cytoplasm (Fig 2E). Both GFP-$SteD_{TMSseG}$ and GFP-$SteD_{TMSseGala13}$ had a similar localisation
116 to mCherry-SseG (Fig 2E). This agrees with previous work showing that the transmembrane domains of
117 SseG direct its localisation in the host cell (9) and demonstrates that this localisation is also independent
118 from membrane integration. Therefore, Region 13 is sufficient to mediate integration of alternative
119 transmembrane domains following targeting to a different membrane compartment.

120 We next examined the process of membrane integration after translocation of SteD by the SPI-2 T3SS.
121 However, $SteD_{ala9}$ and $SteD_{ala13}$ were not stably expressed or translocated by *Salmonella* (Fig S3A).
122 Therefore, we carried out more specific mutagenesis to identify the residues within Regions 9 and 13,
123 whose loss accounts for the properties of $SteD_{ala9}$ and $SteD_{ala13}$. To do this we first tested the ability of
124 GFP-tagged single and double residue alanine substitutions to reduce mMHCII surface levels. All the
125 single residue substitutions were still functional (Fig S3B). The double substitution mutants with the
126 strongest functional impairment ($SteD_{L42A,M43A}$ and $SteD_{S68A,G69A}$, Fig 3A and Fig S3C) were tested for
127 expression in *Salmonella*. Both mutants were translocated into Mel Juso cells and the protein levels
128 were rescued by MG132, demonstrating that they both underwent proteasomal degradation (Fig S3D).
129 Mel Juso cells with similar levels of $SteD_{L42A,M43A}$-HA and $SteD_{S68A,G69A}$-HA as wt SteD-HA had no reduction
130 in mMHCII surface levels (Fig 3B and Fig S3E). Biochemical fractionation revealed that both $SteD_{L42A,M43A}$-
131 HA and $SteD_{S68A,G69A}$-HA were not solubilised by RIPA indicating that they failed to integrate into host
132 cell membranes (Fig 3C). Furthermore, $SteD_{L42A,M43A}$-HA was found in large puncta throughout the host
133 cell cytoplasm, while $SteD_{S68A,G69A}$-HA colocalised with TGN46 (Fig 3D and E). Therefore, following

134 translocation, these mutants recapitulated the non-integration and localisation properties of GFP-
135 $SteD_{ala9}$ and GFP-$SteD_{ala13}$ respectively, indicating that translocated SteD uses the same integration
136 mechanism as ectopically expressed GFP-SteD.

137 Collectively, these results show that following translocation from bacteria, SteD integrates into host cell
138 membranes with a two-step mechanism. First SteD is recruited from the cytoplasm by residues L42 and
139 M43 of Region 9, presumably by interaction with a membrane component(s) and this is followed by
140 integration mediated by residues S68 and G69 of Region 13.

141 SteD integrates into membranes of the early secretory 142 pathway

143 We investigated whether the membrane interaction and integration steps occur at the TGN or if SteD
144 accumulates there after integrating elsewhere in the secretory pathway. To do this we used a
145 doxycycline-regulated promoter to derepress expression of SteD from a mammalian expression plasmid
146 after blocking Golgi trafficking with brefeldin A (BFA). BFA causes the collapse of Golgi membranes into
147 the ER and fusion of TGN membranes with endosomes, thereby separating the early from the late
148 secretory pathway (10,11). When SteD expression was induced in the absence of BFA (dox), it
149 integrated into membranes at both the TGN and MHCII compartments, as expected (Fig 4A-C and Fig
150 S4A). When expressed after Golgi disruption (BFA-dox) SteD still underwent membrane integration (Fig
151 4C) but localised predominantly at the ER and no longer colocalised with TGN46 (Fig 4A and B). GFP-
152 $SteD_{ala13}$ also localised at the ER when expressed after BFA treatment in the presence of MG132 (Fig 4A
153 and B, BFA-dox), demonstrating that the SteD membrane interaction partner re-distributes to the ER
154 after BFA treatment. Therefore, both membrane interaction and integration occur at the ER or Golgi,
155 and not at the TGN.

156 In the presence of BFA, SteD did not cause a significant reduction in mMHCII surface levels (Fig 4D and
157 Fig S4B) and this correlated with a failure to colocalise with mMHCII (Fig S4A). This demonstrates that

158 post-Golgi trafficking is required for SteD to reach MHCII compartments and for SteD function. Indeed,
159 after bleaching the fluorescent signal from GFP-SteD outside of the Golgi area we detected vesicles
160 containing GFP-SteD budding from the Golgi/TGN area by time-lapse microscopy. These vesicles
161 trafficked throughout the cell with some apparently fusing to and budding from other SteD-containing
162 compartments (Video S2 and Fig S4C). Since there is a large amount of colocalisation between GFP-
163 SteD and mMHCII in the periphery of the cell (Bayer-Santos et al., 2016), a substantial proportion of
164 these are likely to be MHCII compartments. The stable association of $SteD_{ala13}$ with the TGN (Fig 2A and
165 Video S1) indicates that post-TGN trafficking of SteD requires membrane integration.

166 Therefore, rather than integrating into the TGN directly, SteD either interacts with an ER or Golgi
167 cisternae component and integrates into these membranes before accumulating at the TGN. SteD is
168 then trafficked to MHCII compartments, and this is required for its function.

169 AP1 mediates trafficking of SteD to MHCII compartments
170 via a sequence resembling an inverted dileucine motif

171 The TGN acts as a sorting platform for the anterograde traffic of protein cargo from the Golgi.
172 Transmembrane cargo proteins frequently use short linear motifs known as sorting signals in their
173 cytoplasmic tails. Sorting signals are recognised by cytoplasmic adaptor proteins, including
174 heterotetrameric AP complexes, allowing concentration of cargo into vesicles targeted to specific
175 membrane compartments (12). In the absence of a sorting signal, proteins traffic constitutively from
176 the TGN to the PM (13). To determine if SteD interacts with an AP complex we used
177 coimmunoprecipitation experiments after chemical crosslinking with dithiobis(succinimidyl
178 propionate) (DSP), which has been shown to be effective for detecting transient interactions between
179 transmembrane proteins and cytoplasmic interaction partners (14). Ectopically expressed GFP-SteD
180 was immunoprecipitated from Mel Juso cell lysates using GFP-trap beads and proteins were subjected
181 to immunoblotting with antibodies against specific subunits of the AP1, 2 or 3 complexes. GFP-tagged

182 SseG was used as a negative control. A small amount of AP1 interacted specifically and reproducibly
183 with GFP-SteD (Fig 5A and B) but not GFP-SseG.

184 AP1 regulates the trafficking of protein cargo between the TGN and endosomes (15). To test whether
185 AP1 is involved in trafficking of SteD to MHCII compartments we used siRNA to knock down the β
186 subunit of AP1 in Mel Juso cells expressing GFP-tagged SteD (Fig 5C). AP1 knockdown had no noticeable
187 effect on cellular mMHCII signal but caused a significant reduction in colocalisation between GFP-SteD
188 and MHCII compartments when compared to mock-treated cells or knockdown of AP2 and AP3 (Fig 5D
189 and E). Despite this reduced colocalisation, knockdown of AP1 had no detectable effect on SteD-
190 dependent reduction of mMHCII surface levels (Fig S5A). While there was no detectable increase in
191 GFP-SteD at the PM (Fig S5B) we conclude that under these conditions a small proportion of SteD is still
192 able to interact with MHCII either intracellularly or at the PM.

193 We next tested whether there is information in the N- or C-terminal cytoplasmic tails of SteD that is
194 required for its AP1-mediated trafficking. Truncation mutants of GFP-SteD lacking the C-terminal tail or
195 most of the N-terminal tail (Fig 6A and Fig S6A) underwent membrane integration as assessed by
196 biochemical fractionation (Fig 6B). Truncation of the C-terminal tail (GFP-SteD$_{1-102}$) did not affect
197 localisation at the TGN and MHCII compartments (Fig 6C and Fig S6B). On the other hand, an SteD
198 truncation lacking most of the N-terminal cytoplasmic tail (GFP-SteD$_{37-111}$) had reduced localisation at
199 MHCII compartments (Fig 6C). Furthermore, and in contrast to AP1 depletion, truncation of the N-
200 terminal tail resulted in a dramatic increase in the proportion of fluorescence signal at the cell surface
201 and a decrease in fluorescence signal at the TGN (Fig 6C and D and Fig S6B). The continuous distribution
202 of fluorescence signal at the cell surface along with the ability to integrate into the membrane implies
203 a PM localisation. Remarkably, a construct lacking most of the N-terminal tail and the C-terminal tail
204 (GFP-SteD$_{37-102}$), leaving just 65 residues comprising the two transmembrane domains separated by the
205 luminal loop and containing Regions 9 and 13, also integrated efficiently into host cell membranes (Fig
206 6A and B) and along with GFP-SteD$_{37-111}$, localised at the TGN as well as the PM (Fig 6C and D).

207 To test whether the PM localisation was due to traffic from the TGN, we used the photoconvertible
208 fluorescent protein mEos, which converts from green to red fluorescence upon activation with UV light,
209 to specifically activate SteD at the Golgi and track its subsequent fate. As expected, vesicles containing
210 mEos-SteD travelled from the Golgi throughout the cell cytoplasm (Video S3 and Fig S6C). In contrast,
211 vesicles containing the N-terminal truncation of SteD trafficked to the periphery of the cell, where the
212 fluorescent signal dissipated (Video S3 and Fig S6C), presumably as a result of vesicle fusion and lateral
213 dilution of the fluorescent signal in the PM. These results suggest the presence of a sorting signal in the
214 N-terminal tail of SteD that directs traffic from the TGN to MHCII compartments and whose absence
215 results in mis-trafficking to the PM.

216 There are two well-characterised sorting signals that interact with AP complexes: the tyrosine motif,
217 YXXΦ, where Φ is a large hydrophobic residue, and the dileucine motif, [DE]XXXL[LI], with one or more
218 acidic residues upstream from two leucines (X indicates any residue in both motifs) (16). No series of
219 residues in SteD match the consensus of either motif, however sequences resembling both motifs are
220 present in inverted orientations in the N terminal tail. F32, N33, A34 and Y35 resemble an inverted
221 tyrosine motif, and are within a region necessary for SteD function, as determined by alanine scanning
222 mutagenesis (Region 7, Fig S1A) (4). A double alanine substitution of F32 and Y35 ($SteD_{F32A,Y35A}$) was
223 sufficient to inhibit the effect of SteD on mMHCII surface levels to the same level as $SteD_{ala7}$ following
224 ectopic expression or translocation from *Salmonella* (Fig 7A and Fig S7A and B). Alanine substitution of
225 the remaining residues within Region 7, N33 and G36, had no effect on SteD function (Fig S7A).
226 However, the F32A,Y35A double mutation had no noticeable effect on the localisation of SteD (Fig S7C-
227 E) and did not prevent interaction of SteD with AP1 when expressed ectopically (Fig S7F and G). This
228 rules out the involvement of these residues in AP1-dependent transport and suggests that they
229 contribute to SteD function in other ways.

230 Amino acids L13 and L14 of SteD, followed by P, P, S and then by two charged residues (E18, R19),
231 resemble an inverted dileucine motif (Fig 7A). Alanine substitution of the leucines alone ($SteD_{L13A,L14A}$-

232 HA) had no noticeable effect on localisation of SteD after translocation from *Salmonella* (Fig S7H).
233 However, further alanine substitution of the two charged residues (E18 and R19) (SteD$_{L13A,L14A,E18A,R19A}$-
234 HA) significantly increased the proportion of HA signal at the cell surface (Fig 7B and C) and reduced
235 the level of colocalisation with mMCHII (Figs 7B and D) when compared to wt SteD-HA. An increase in
236 cell surface signal and decrease in colocalisation with mMHCII was also detected for ectopically
237 expressed GFP-SteD$_{L13A,L14A,E18A,R19A}$ compared to wt GFP-SteD (Fig S7C-E). Therefore, this quadruple
238 substitution mutation recapitulated the mis-localisation phenotype of the N-terminal truncation of
239 GFP-SteD$_{37-111}$. Furthermore, mMHCII surface levels were significantly higher after translocation of
240 SteD$_{L13A,L14A,E18A,R19A}$-HA compared to wt SteD-HA (Fig 7E). Mis-localisation of SteD$_{L13A,L14A,E18A,R19A}$ did not
241 prevent interaction with TMEM127 (Fig S7F and G). This suggests that SteD interacts with TMEM127 at
242 the ER, Golgi or TGN through which TMEM127 passes (17), and is consistent with other work showing
243 that SteD can interact with TMEM127 in the absence of mMHCII (6). Finally, interaction between
244 SteD$_{L13A,L14A,E18A,R19A}$ and AP1 was reduced significantly after translocation from *Salmonella* (Fig 7F and
245 G) and ectopic expression (Fig S7F and G). Therefore, these residues are required for interaction with
246 AP1, resulting in trafficking of SteD from the TGN to MHCII compartments, which is required for SteD
247 function.

248 # Discussion

249 Many bacterial type III secretion systems effectors are specifically targeted to organelles and
250 membranes within the infected cell and interference with localisation processes frequently results in
251 their loss of function (18–21). The targeting mechanisms of transmembrane effectors, which post-
252 translationally integrate into specific host cell membranes, is not well understood. The majority of
253 translocated SteD accumulates at the TGN but its substrates including mature MHCII are located in
254 endosomal compartments and at the PM, raising the question of how SteD reaches these sites. In this
255 work we used site directed mutagenesis of SteD to identify distinct regions of SteD that are required
256 for initial targeting to the ER/Golgi, membrane integration and for AP1-mediated trafficking to MHCII
257 compartments (Fig 8). This demonstrates how a bacterial virulence protein can enter the membrane
258 network of the eukaryotic cell and hijack a vesicular trafficking pathway to regulate its localisation and
259 ultimately its function.

260 Apart from SteD, a few other effectors have been reported to undergo integration into membranes of
261 the secretory pathway. Tir, a conserved T3SS effector of pathogenic *E. coli* with a similar membrane
262 topology to SteD, localises to the PM where it induces actin pedestals and enables tight attachment of
263 extracellular bacteria by binding to the bacterial surface protein, Intimin (22). Enterohemorrhagic *E.*
264 *coli* (EHEC) Tir was also shown to localise at the Golgi network by immunofluorescence and
265 immunoelectron microscopy (23). Exposure of host cells to BFA prior to infection with EHEC prevented
266 pedestal formation, suggesting that Tir, like SteD must first pass through the Golgi before reaching its
267 site of action at the PM (23). NleA/EspI, another EHEC effector, contains two putative transmembrane
268 domains and was shown by triton-dependent solubilisation following fractionation of infected host cells
269 to integrate into membranes (24). NleA/EspI localises to the Golgi through interaction with the COPII
270 component, Sec24 (25). This interaction stabilises COPII at the Golgi leading to a reduction in general
271 protein secretion (26). Interestingly, overexpressed NleA interferes with MHCII invariant chain
272 transport and it might thereby also affect antigen presentation (27).

273 Transmembrane effectors have been suggested to integrate into their target membranes either
274 indirectly, by lateral transfer during translocation into the membrane containing the T3SS translocon,
275 followed by membrane fission and vesicular trafficking to another destination, or directly, following
276 translocation of the effector into the cytoplasm (3). In the case of SteD, indirect targeting could result
277 from vesicles containing SteD trafficking from the SCV to the Golgi. However, direct integration is more
278 likely for three reasons. First, ectopically expressed GFP-SteD mimics the bacterial translocated effector
279 with respect to Golgi localisation, membrane integration and action on mMHCII (4), (and this work),
280 showing that an SCV membrane and translocon are not required for these processes. Second, Golgi
281 localisation is independent from membrane integration, as demonstrated by SteD mutants incapable
282 of integration, showing that this localisation does not require vesicular trafficking. Third, mutants
283 incapable of either membrane recruitment or integration accumulated within the host cell cytoplasm
284 following translocation.

285 We propose that SteD is recruited to its target membrane from the cytoplasm through interaction of
286 Region 9 with a protein or lipid, or a combination of components at the cytoplasmic face of the ER
287 and/or the Golgi cisternae. Identification of the host interaction partner(s) and its involvement in
288 membrane integration is needed to better define the process of SteD integration. Following
289 recruitment, SteD undergoes membrane integration by a mechanism involving Region 13, and
290 specifically S68 and G69. The ability of Region 13 to mediate integration of the transmembrane regions
291 of SseG shows that this mechanism is non-specific. As glycine residues have a high propensity to induce
292 a turn between two transmembrane helices (28), G69 could enable the formation of a hairpin-like
293 structure and hence facilitate the conformation required for integration upon interaction with the
294 membrane. A two-step membrane integration process is consistent with the mechanism of integration
295 proposed for Tir, whereby a region close to the transmembrane domain binds peripherally to the
296 membrane, resulting in a conformational change enabling the hydrophobic domains to adopt an
297 orientation that drives membrane insertion (Race et al., 2006). Insertion of purified Tir into

298 reconstituted membrane vesicles does not require host proteins but does depend on sphingomyelin
299 (29), which is made at the ER and Golgi and enriched at the PM (30).

300 Microscopic analysis of the non-membrane integrating $SteD_{ala13}$ mutant showed that it remained
301 confined to the Golgi region, indicating that SteD must be in its membrane-integrated state to undergo
302 onward post-TGN transport. SteD thus resembles transmembrane cargo proteins that are recognised
303 for vesicular traffic by adaptor proteins via sorting signals in their cytoplasmic tails, such as the dileucine
304 motif [DE]XXXL[LI]. It is therefore interesting that the LLPPSER sequence required for transport of SteD
305 to MHCII compartments resembles an inverted dileucine motif. This could represent an example of
306 effector mimicry by convergent evolution. However, individual substitution of either leucine inactivates
307 mammalian [DE]XXXL[LI] sorting signals (12), whereas the localisation of the $SteD_{L13A,L14A}$-HA double
308 mutant was similar to that of wt SteD. Furthermore, although inverted leucine-containing motifs can
309 mediate substrate recognition in other proteins (31) it is not clear whether SteD's LLPPSER sequence
310 interacts directly with the AP1 binding site or whether other proteins are involved in the process.
311 Further biochemical and structural studies are required to determine the molecular details of the
312 SteD/AP1 interface.

313 Other intracellular pathogen proteins have been shown to interact with adaptor proteins through
314 canonical dileucine motifs. The Coxiella burnetii T4SS effector CvpA interacts with AP2 via three
315 dileucine motifs (EESKLL, RHINLL and EIQQLL) and re-routes endocytic compartments to the pathogen-
316 containing vacuole (32). HIV-1 proteins Nef and Vpu interact with host adaptor protein complexes via
317 ENTSLL and ELSALV sequences respectively, resulting in the redistribution of cell surface proteins
318 involved in cellular immunity (33,34). By re-routing protein cargo or trafficking pathways these proteins
319 aid pathogen replication. On the other hand, by localising within membranes of the secretory pathway
320 and by virtue of its LLPPSER post-TGN sorting sequence, SteD resembles classical transmembrane
321 protein cargo.

322 Through interaction with AP1, SteD exploits an established host cell trafficking pathway between the
323 TGN and endosomes (15,35). Indeed, AP1 mediates delivery of invariant chain-bound MHCII complexes
324 from the TGN to MHCII compartments (36). Although blocking MHCII compartment localisation by
325 expressing SteD after Golgi disruption totally prevented SteD function, disrupting its post-TGN traffic
326 through mutation of the LLPPSER sequence or AP1 knockdown only partially disrupted or did not affect
327 SteD function, respectively. It is possible that a small but functionally significant amount of SteD is still
328 able to reach MHCII compartments in these conditions. Alternatively, in the case of $SteD_{L13A,L14A,E18A,R19A}$,
329 this could be due to the partial functionality of SteD at the PM, where it might also come into contact
330 with mMHCII. The differences between AP1 knockdown and mutation of the dileucine sequence in
331 relation to SteD localisation and functionality could be due to incomplete AP1 knockdown or to a
332 redundancy in interaction of wt SteD with other adaptors.

333 The dependence on AP1 for trafficking to MHCII compartments might well create a rate-limiting step
334 for post TGN SteD traffic, explaining the accumulation of SteD at the TGN. This might also provide a
335 source of SteD to replenish that which is lost by degradation as a result of ubiquitination by the
336 TMEM127/WWP2 machinery (6).

337 The mutational dissection of SteD described in this and our previous work enables the following
338 functional regions of the protein to be defined: L13, L14, E18 and R19, an inverted dileucine motif-like
339 sequence involved in post TGN transport to MHCII compartments (this work); K24 undergoes
340 ubiquitination which contributes to the ability of SteD to induce ubiquitination of mMHCII (6); L42 and
341 M43, recruitment to the ER/Golgi (this work); S68 and G69, integration into membranes (this work); 5
342 – transmembrane regions, intramembrane interaction with TMEM127 (6); Residues in the C-terminal
343 tail, interaction with MHCII (4). Taken together, this reveals a remarkable level of functional complexity
344 within this small bacterial protein, resulting in the disruption of the adaptive immune response by
345 reducing surface levels of at least three key proteins, CD97 (5), CD86/B7.2 (4) and mMHCII (4).

346 # Materials and Methods

347 ## Bacterial strains, plasmids and antibodies

348 *Salmonella enterica* serovar Typhimurium (14028s) wild-type and all mutant strains are listed in Table
349 S1. Bacteria were grown in Luria–Bertani (LB) medium supplemented with carbenicillin (50 µg ml^{-1}) or
350 kanamycin (50 µg ml^{-1}) as appropriate. All plasmids used are listed in Table S2. All antibodies used are
351 listed in Table S3.

352 ## Cell culture and infection

353 Human Mel Juso cells were maintained in Dulbecco's Modified Eagle Medium (DMEM, Sigma)
354 containing 10% heat-inactivated fetal calf serum (FCS, Gibco) at 37°C in 5% CO_2. When indicated, cells
355 were incubated with DMEM containing MG132 (10 µM, Sigma) or DMSO as a vehicle control (1:1000)
356 for 5 h. To disrupt the Golgi, cells were incubated in DMEM containing BFA (10 µg ml^{-1}, Sigma) for 3 h.

357 Mel Juso cells were infected for 30 min at MOI of 100 with late log-phase *Salmonella* grown in LB. Cells
358 were washed twice with PBS and incubated in fresh medium containing gentamicin (100 µg ml^{-1}) for 1
359 h to kill extracellular bacteria. After 1 h, the antibiotic concentration was reduced to 20 µg ml^{-1}, and the
360 cells were processed 20 h post-invasion (p.i.).

361 For analysis of translocated effectors cells were lysed in 0.1% Triton X-100 and incubated on ice for 15
362 min with vortexing. The post-nuclear supernatant (PNS) was separated from the nuclear pellet and non-
363 lysed *Salmonella* cells by centrifugation.

364 ## Transfection

365 For transient plasmid transfections, plasmids and lipofectamine 2000 were combined and incubated in
366 OptiMEM for 5 min at room temperature before being added to cells. Cells were analysed 16-20 h after
367 plasmid transfection. For siRNA transfections, siRNA and Lipofectamine RNAiMAX (Life Technologies)
368 were combined and incubated in OptiMEM for 5 min at room temperature before being added to cells.
369 AP1B1 siRNA mix (UAGACGAGCUUAUCUGCUA, CCACUCAGGACUCAGAUAA,
370 GGAAGGCUGUGCGUGCUAU, CUAAGGACUUGGACUACUA), AP2M1 siRNA mix

371 (GUUAAGCGGUCCAACAUUU, GCGAGAGGGUAUCAAGUAU, AGUUUGAGCUUAUGAGGUA,
372 GAACCGAAGCUGAACUACA), AP3D1 siRNA mix (CUACAGGGCUCUGGAUAUU,
373 GGACGAGGCAAAAUACAUA, GAAGGACGUUCCCAUGGUA, CAAAGUCGAUGGCAUUCGG) and Scrambled
374 siRNA mix (UGGUUUACAUGUCGACUAA, UGGUUUACAUGUUGUGUGA, UGGUUUACAUGUUUUCUGA,
375 UGGUUUACAUGUUUUCCUA) were purchased from Dharmacon and used at 5 pmol. Cells were diluted
376 24 h after siRNA transfection and analysed 3 days after siRNA transfection.

377 Induced expression of SteD

378 To regulate GFP-SteD expression a Tet-on system was used. Mel Juso cells stably expressing the Tet
379 Repressor from the pcDNA^{TM} 6/TR vector (Life Technologies) were made following the manufacturer's
380 instructions. The vector was linearised and transfected into Mel Juso cells as described above.
381 Expressing cells were selected with 10 µg ml^{-1} Blasticidin. A clonal population was selected based on
382 maximum repressor expression. GFP-SteD was cloned into the pcDNA 4/TO vector (Life Technologies)
383 following the manufacturer's instructions (Table S2) and transiently transfected into the repressor-
384 expressing cells. Expression was induced with DMEM containing 1 µg ml^{-1} doxycycline for 4 h.

385 Flow cytometry

386 Surface levels of mMHCII were measured following infection or transfection of Mel Juso cells as
387 described previously (4) with minor modifications. In brief, Mel Juso cells were detached using 2 mM
388 EDTA in PBS. All antibodies were diluted in FACS buffer (5% FCS and 1 mM EDTA in PBS). See Table S3
389 for information on primary antibodies; secondary antibodies were purchased from Life Technologies,
390 UK. Cells were labelled with mouse anti-HLA-DR (mMHCII) at 1:300 for 30 min on ice, washed in cold
391 PBS, then labelled with Alexa Fluor 647 donkey anti-mouse at 1:300 for 30 min on ice. For detection of
392 intracellular *Salmonella* and translocated HA-tagged SteD, cells were fixed in 3.7% paraformaldehyde
393 for 1 h at room temperature and permeabilised with 0.1% Triton X-100 in FACS buffer for 10 min at
394 room temperature. Subsequently, cells were labelled with goat anti-*Salmonella* CSA-1 at 1:500 and rat
395 anti-HA at 1:200 antibodies for 30 min on ice. Cells were washed in cold PBS, then labelled with Alexa
396 Fluor 555 donkey anti-goat and Alexa Fluor 488 donkey anti-rat antibodies both at 1:300 for 30 min on

397 ice. Surface levels of mMHCII were calculated as geometric mean of infected cells or GFP-positive
398 cells/geometric mean of uninfected cells or GFP-negative cells x 100. Data were acquired using Calibur
399 or Fortessa flow cytometer (BD Biosciences) and analysed using FlowJo v10 software.

400 Membrane fractionation

401 Mel Juso cells expressing GFP-tagged SteD variants or infected with *Salmonella* expressing HA-tagged
402 SteD variants were collected and lysed in homogenization buffer (250 mM sucrose, 3 mM imidazole
403 (pH 7.4), and 1 mM phenylmethylsulfonyl fluoride (PMSF)) by mechanical disruption using a Dounce
404 homogenizer. The post-nuclear supernatant was collected after centrifugation at 1,800 *g* for 15 min
405 and split into three samples. The membrane fraction was pelleted and separated from the soluble
406 fraction in each sample by centrifugation at 100,000 *g* for 1 h at 4°C. One membrane pellet was used
407 as the total membrane sample. To remove peripherally-associated proteins, the second membrane
408 pellet was resuspended in 2.5 M urea and incubated for 15 min on ice followed by centrifugation at
409 100,000 *g* for 1 h at 4°C. This yielded a pellet containing integral membrane proteins and a supernatant
410 containing peripherally-associated membrane proteins. To solubilise integral membrane proteins the
411 third membrane pellet was resuspended in RIPA buffer (150 mM NaCl, 1% Triton X-100, 0.5% sodium
412 doxycholate, 0.1% SDS and 50 mM Tris-Cl (pH 8.0)) and incubated on ice for 15 min with vortexing
413 followed by centrifugation at 100,000 *g* for 1 h at 4°C. This yielded a pellet containing protein
414 aggregates and a supernatant containing integral membrane proteins. All samples were analysed by
415 SDS PAGE and immunoblotting. The MHCII α chain was used as an integral membrane protein control.
416 Actin was used as a soluble protein control. Golgin-97 was used as a peripherally-associated membrane
417 protein control.

418 Immunofluorescence microscopy

419 Cells were seeded onto coverslips and infected or transfected as described above. Cells were washed
420 in PBS, fixed in 3% paraformaldehyde in PBS for 15 min at room temperature, then the
421 paraformaldehyde was quenched by incubation with 50 mM NH_4Cl for 10 min. All antibodies were
422 diluted in 10% horse serum (Sigma) and 0.1% saponin (Sigma) in PBS. Coverslips were washed in 0.1%

423 saponin in PBS then incubated with appropriate primary antibodies for 1 h at room temperature,
424 washed in 0.1% saponin in PBS, then incubated with secondary antibodies for 1 h at room temperature.
425 Finally, coverslips were incubated with 0.5 µg ml^{-1} DAPI (Invitrogen) for 5 min, washed in 0.1% saponin
426 in PBS then mounted onto glass slides using Aqua-Poly/Mount (Polysciences, Inc.). See Table S3 for
427 information on primary antibodies and dilutions used. Secondary antibodies were purchased from Life
428 Technologies, UK.

429 Confocal microscopy and live-cell imaging

430 All coverslips were imaged at room temperature using a confocal laser scanning microscope (LSM 710,
431 Carl Zeiss) equipped with a Plan Apochromat 63x (Carl Zeiss) oil-immersion objective. For live imaging,
432 cells were seeded in dishes (Matek) with an embedded glass cover slip. Prior to imaging, DMEM was
433 replaced with FluoroBrite (Gibco) containing 10% FCS (Gibco), 40 mM Hepes (Sigma) and 2 mM L-
434 Glutamine (Sigma). Live cells were maintained at 37 °C in a heated chamber. Protein expression was
435 blocked with cycloheximide (50 µg ml^{-1}) for 1 h before photobleaching. Photobleaching of GFP was
436 performed using a 488 nm laser. Photoconversion of mEos was performed using a 405 nm laser.

437 Image analysis

438 Quantitative analyses of SteD at the TGN or plasma membrane were done using CellProfiler software
439 (37). Nuclei were segmented from the DAPI signal. TGN objects were segmented using TGN46 labelling,
440 and the outline of cells were segmented using background labelling from TGN46. Tertiary plasma
441 membrane objects were segmented by expanding and shrinking the cell object by 4 pixels
442 (corresponding to 0.5 µm) and then subtracting the shrunken cell from the expanded cell. Fluorescence
443 intensity measurements were made after extracellular background subtraction using a rolling ball
444 radius of 200 pixels (corresponding to 26.4 µm). Non-transfected or uninfected cells were excluded
445 from the analysis based on a threshold. The mean intensity of the SteD signal was measured from TGN
446 and plasma membrane segmentation masks. The log_{10} of the ratio of the segmented signal over the
447 total cellular signal was calculated for each cell.

448 Pearson's correlation coefficient was calculated using ImageJ software. The extracellular background
449 was subtracted from images using the Background Subtraction function in ImageJ, with a rolling ball
450 radius equal to 200 pixels or 26.4 µm. Pearson's correlation coefficient values were obtained from
451 individual cells using the Coloc 2 ImageJ plugin (http://imagej.net/Coloc_2). Mander's overlap
452 coefficient was calculated using ImageJ software to measure the proportion of colocalising pixels
453 between two punctate signals. The extracellular background was subtracted from images as above.
454 Local background was corrected by subtracting the median intensity of a 10 x 10 pixel region
455 surrounding each pixel. Non-specific fluorescence was then subtracted using values measured from
456 unlabelled cells. The images were then converted to binary and the Mander's overlap coefficient was
457 measured from individual cells using the Coloc 2 imageJ plugin.

458 Immunoprecipitation

459 Mel Juso cells expressing GFP-tagged SteD variants or infected with *Salmonella* expressing HA-tagged
460 SteD variants as indicated were harvested in cold PBS, washed and then resuspended in 2 mM
461 dithiobis(succinimidyl propionate) (DSP) (Sigma) and incubated for 2 h at 4°C to crosslink intracellular
462 proteins before cell lysis. Cells were pelleted and resuspended in 20 mM Tris (pH 8.0) for 15 min at
463 room temperature to stop the crosslinking reaction. Cells were lysed in lysis buffer (5% glycerol, 0.5%
464 Triton X-100, 1 mM PMSF in PBS) for 30 min at 4°C. The post-nuclear supernatant was obtained by
465 centrifugation at 16,000 *g* for 10 min. Proteins were immunoprecipitated by incubation with anti-HA
466 sepharose beads (Pierce) or anti-GFP-Trap beads (ChromoTek) for 2 h at 4°C. Immunoprecipitates were
467 washed four times with lysis buffer and boiled in SDS buffer containing 2.5% β-mercaptoethanol and
468 400 mM DTT before analysis by SDS-PAGE and immunoblotting. Densitometry measurements were
469 carried out using Image Lab software (Bio-Rad).

470 Acknowledgements

471 The authors would like to thank Teresa Thurston, Ondrej Cerny and Peter Hill for helpful comments
472 on the manuscript. We are grateful to Jacques Neefjes for providing Mel Juso cells. mCherry-ER-3 was

a gift from Michael Davidson (Addgene plasmid 55041), mEos3.2-Tubulin-C-18 was a gift from Michael Davidson (Addgene plasmid 57484). This work was supported by an Investigator Award from the Wellcome Trust (209411/Z/17/Z) to D.W.H.

References

1. Escoll P, Mondino S, Rolando M, Buchrieser C. Targeting of host organelles by pathogenic bacteria: a sophisticated subversion strategy. Nat Rev Microbiol. 2016 Jan;14(1):5–19.

2. Hicks SW, Galán JE. Exploitation of eukaryotic subcellular targeting mechanisms by bacterial effectors. Nat Rev Microbiol. 2013 May;11(5):316–26.

3. Krampen L, Malmsheimer S, Grin I, Trunk T, Lührmann A, de Gier J-W, et al. Revealing the mechanisms of membrane protein export by virulence-associated bacterial secretion systems. Nat Commun. 2018;9(1):3467.

4. Bayer-Santos E, Durkin CH, Rigano LA, Kupz A, Alix E, Cerny O, et al. The Salmonella Effector SteD Mediates MARCH8-Dependent Ubiquitination of MHC II Molecules and Inhibits T Cell Activation. Cell Host Microbe. 2016 Nov 9;20(5):584–95.

5. Cerny O, Godlee C, Tocci R, Cross NE, Shi H, Williamson JC, et al. CD97 stabilises the immunological synapse between dendritic cells and T cells and is targeted for degradation by the Salmonella effector SteD. PLoS Pathog. 2021;17(7):e1009771.

6. Alix E, Godlee C, Cerny O, Blundell S, Tocci R, Matthews S, et al. The Tumour Suppressor TMEM127 Is a Nedd4-Family E3 Ligase Adaptor Required by Salmonella SteD to Ubiquitinate and Degrade MHC Class II Molecules. Cell Host Microbe. 2020 Jul 8;28(1):54-68.e7.

7. Godlee C, Cerny O, Durkin CH, Holden DW. SrcA is a chaperone for the Salmonella SPI-2 type three secretion system effector SteD. Microbiology. 2019;165(1):15–25.

8. Kopito RR. Aggresomes, inclusion bodies and protein aggregation. Trends Cell Biol. 2000 Dec 1;10(12):524–30.

9. Salcedo SP, Holden DW. SseG, a virulence protein that targets Salmonella to the Golgi network. EMBO J. 2003 Oct 1;22(19):5003–14.

10. Lippincott-Schwartz J, Yuan LC, Bonifacino JS, Klausner RD. Rapid redistribution of Golgi proteins into the ER in cells treated with brefeldin A: evidence for membrane cycling from Golgi to ER. Cell. 1989 Mar 10;56(5):801–13.

11. Wood SA, Park JE, Brown WJ. Brefeldin A causes a microtubule-mediated fusion of the trans-Golgi network and early endosomes. Cell. 1991 Nov 1;67(3):591–600.

12. Bonifacino JS, Traub LM. Signals for sorting of transmembrane proteins to endosomes and lysosomes. Annu Rev Biochem. 2003;72:395–447.

13. Stalder D, Gershlick DC. Direct trafficking pathways from the Golgi apparatus to the plasma membrane. Semin Cell Dev Biol. 2020;107(January):112–25.

14. Jafferali MH, Vijayaraghavan B, Figueroa RA, Crafoord E, Gudise S, Larsson VJ, et al. MCLIP, an effective method to detect interactions of transmembrane proteins of the nuclear envelope in live cells. Biochim Biophys Acta. 2014 Oct;1838(10):2399–403.

15. Hirst J, Borner GHH, Antrobus R, Peden AA, Hodson NA, Sahlender DA, et al. Distinct and overlapping roles for AP-1 and GGAs revealed by the “knocksideways” system. Curr Biol. 2012 Sep 25;22(18):1711–6.

16. Robinson MS. Adaptable adaptors for coated vesicles. Trends Cell Biol. 2004 Apr;14(4):167–74.

515 17. Qin Y, Yao L, King EE, Buddavarapu K, Lenci RE, Chocron ES, et al. Germline mutations in
516 TMEM127 confer susceptibility to pheochromocytoma. Nat Genet. 2010 Mar;42(3):229–33.

517 18. Boucrot E, Beuzón CR, Holden DW, Gorvel J-P, Méresse S. Salmonella typhimurium SifA
518 effector protein requires its membrane-anchoring C-terminal hexapeptide for its biological
519 function. J Biol Chem. 2003 Apr 18;278(16):14196–202.

520 19. Hicks SW, Charron G, Hang HC, Galán JE. Subcellular targeting of Salmonella virulence proteins
521 by host-mediated S-palmitoylation. Cell Host Microbe. 2011 Jul 21;10(1):9–20.

522 20. Lau N, Haeberle AL, O'Keeffe BJ, Latomanski EA, Celli J, Newton HJ, et al. SopF, a
523 phosphoinositide binding effector, promotes the stability of the nascent Salmonella-containing
524 vacuole. PLoS Pathog. 2019;15(7):e1007959.

525 21. Salomon D, Guo Y, Kinch LN, Grishin N V., Gardner KH, Orth K. Effectors of animal and plant
526 pathogens use a common domain to bind host phosphoinositides. Nat Commun. 2013;4:2973.

527 22. Frankel G, Phillips AD, Trabulsi LR, Knutton S, Dougan G, Matthews S. Intimin and the host cell-
528 -is it bound to end in Tir(s)? Trends Microbiol. 2001 May;9(5):214–8.

529 23. Mao C, Gu J, Wang H-G, Fang Y, Yang P, Tang B, et al. Translocation of enterohemorrhagic
530 Escherichia coli effector Tir to the plasma membrane via host Golgi apparatus. Mol Med Rep.
531 2017 Aug;16(2):1544–50.

532 24. Gruenheid S, Sekirov I, Thomas NA, Deng W, O'Donnell P, Goode D, et al. Identification and
533 characterization of NleA, a non-LEE-encoded type III translocated virulence factor of
534 enterohaemorrhagic Escherichia coli O157:H7. Mol Microbiol. 2004;51(5):1233–49.

535 25. Thanabalasuriar A, Bergeron J, Gillingham A, Mimee M, Thomassin J-L, Strynadka N, et al.
536 Sec24 interaction is essential for localization and virulence-associated function of the bacterial
537 effector protein NleA. Cell Microbiol. 2012 Aug;14(8):1206–18.

538 26. Kim J, Thanabalasuriar A, Chaworth-Musters T, Fromme JC, Frey EA, Lario PI, et al. The
539 bacterial virulence factor NleA inhibits cellular protein secretion by disrupting mammalian
540 COPII function. Cell Host Microbe. 2007 Sep 13;2(3):160–71.

541 27. Cloutier M, Gauthier C, Fortin JS, Genève L, Kim K, Gruenheid S, et al. ER egress of invariant
542 chain isoform p35 requires direct binding to MHCII molecules and is inhibited by the NleA
543 virulence factor of enterohaemorrhagic Escherichia coli. Hum Immunol. 2015;76(4):292–6.

544 28. Monné M, Hermansson M, von Heijne G. A turn propensity scale for transmembrane helices. J
545 Mol Biol. 1999 Apr 23;288(1):141–5.

546 29. Race PR, Lakey JH, Banfield MJ. Insertion of the enteropathogenic Escherichia coli Tir virulence
547 protein into membranes in vitro. J Biol Chem. 2006 Mar 24;281(12):7842–9.

548 30. Ridgway ND. Interactions between metabolism and intracellular distribution of cholesterol and
549 sphingomyelin. Biochim Biophys Acta. 2000 Apr 12;1484(2–3):129–41.

550 31. Tintignac LA, Lagirand J, Batonnet S, Sirri V, Leibovitch MP, Leibovitch SA. Degradation of
551 MyoD mediated by the SCF (MAFbx) ubiquitin ligase. J Biol Chem. 2005 Jan 28;280(4):2847–
552 56.

553 32. Larson CL, Beare PA, Howe D, Heinzen RA. Coxiella burnetii effector protein subverts clathrin-
554 mediated vesicular trafficking for pathogen vacuole biogenesis. Proc Natl Acad Sci U S A. 2013

555 Dec 3;110(49):E4770-9.

556 33. Chaudhuri R, Lindwasser OW, Smith WJ, Hurley JH, Bonifacino JS. Downregulation of CD4 by
557 human immunodeficiency virus type 1 Nef is dependent on clathrin and involves direct
558 interaction of Nef with the AP2 clathrin adaptor. J Virol. 2007 Apr;81(8):3877–90.

559 34. Jia X, Weber E, Tokarev A, Lewinski M, Rizk M, Suarez M, et al. Structural basis of HIV-1 Vpu-
560 mediated BST2 antagonism via hijacking of the clathrin adaptor protein complex 1. Elife. 2014
561 Apr 29;3(3):e02362.

562 35. Tan JZA, Gleeson PA. Cargo Sorting at the trans-Golgi Network for Shunting into Specific
563 Transport Routes: Role of Arf Small G Proteins and Adaptor Complexes. Cells. 2019;8(6):531.

564 36. Neefjes J, Jongsma MLM, Paul P, Bakke O. Towards a systems understanding of MHC class I
565 and MHC class II antigen presentation. Nat Rev Immunol. 2011 Nov 11;11(12):823–36.

566 37. Carpenter AE, Jones TR, Lamprecht MR, Clarke C, Kang IH, Friman O, et al. CellProfiler: image
567 analysis software for identifying and quantifying cell phenotypes. Genome Biol.
568 2006;7(10):R100.

569

570 # Figure Legends

571 ## Fig 1 – Two regions of SteD are required for membrane integration

572 (A) Amino acid sequence of SteD showing predicted transmembrane domains. The N- and C-terminal
573 residues are highlighted in blue and red respectively. The residues substituted to alanines in $SteD_{ala9}$
574 and $SteD_{ala13}$ mutants are highlighted in yellow and orange respectively.

575 (B) Protein immunoblots of whole-cell lysates derived from Mel JuSo cells expressing GFP-SteD (wt or
576 mutants) and treated with MG132 or DMSO carrier. UB – ubiquitin.

577 (C) mMHCII surface levels of Mel JuSo cells expressing GFP or GFP-SteD (wt or mutants) and treated
578 with MG132. Cells were analysed by flow cytometry and amounts of surface mMHCII in GFP-positive
579 cells are expressed as a percentage of GFP-negative cells in the same sample. Mean of three
580 independent experiments done in duplicate ± SD. Data were analysed by one-way ANOVA followed by
581 Dunnett's multiple comparison test, *** $p<0.001$, n.s. – not significant.

582 (D) Protein immunoblots of membrane fractionation samples from Mel Juso cells expressing GFP-SteD
583 (wt or mutants) and treated with MG132. Samples were taken from the pellet (P) and supernatant (S)
584 of the total sample, after urea wash and after RIPA wash.

585 ## Fig 2 – Recruitment of SteD to the TGN is independent from membrane
586 ## integration

587 (A) Representative confocal immunofluorescence microscopy images of Mel JuSo cells expressing
588 GFP-SteD (wt or mutants) after MG132 treatment. Cells were fixed and processed for
589 immunofluorescence microscopy by labelling for the TGN (TGN46, red), and DNA (DAPI, blue). Scale
590 bar – 10 µm.

591 (B) Quantification of GFP at the TGN of cells represented in Fig 2A. The fluorescence intensity of the
592 GFP signal at the TGN was measured in relation to total cellular fluorescence. Data are representative
593 of three independent experiments. Each dot represents the value for one cell. Mean ± SD. The log_{10}
594 fold change of the data were analysed by one-way ANOVA followed by Dunnett's multiple comparison
595 test, *** $p<0.001$, * $p<0.05$.

596 (C) Schematic of SteD chimera with transmembrane domains of SseG.

597 (D) Protein immunoblots of membrane fractionation samples from Mel Juso cells expressing GFP-SteD
598 (wt or chimeric mutants) and treated with MG132. Samples were taken from the pellet (P) and
599 supernatant (S) of the total sample, after urea wash and after RIPA wash.

600 (E) Representative confocal immunofluorescence microscopy images of Mel JuSo cells expressing
601 GFP-SteD (wt or chimeric mutants) and mCherry-SseG after MG132 treatment. Cells were fixed and
602 processed for immunofluorescence microscopy by labelling for the TGN (TGN46, grey), and DNA
603 (DAPI, blue). Scale bar – 10 µm.

604 ## Fig 3 – Membrane integration following translocation

605 (A) Amino acid sequence of SteD showing predicted transmembrane domains. The N- and C-terminal
606 residues are highlighted in blue and red respectively. The residues substituted to alanines in
607 $SteD_{L42A,M43A}$ and $SteD_{S68A,G69A}$ mutants are highlighted in yellow and orange respectively.

608 (B) mMHCII surface levels of Mel JuSo cells infected with *ΔsteD Salmonella* carrying a plasmid
609 expressing SteD-HA (wt or mutants) or SPI-2 null *ΔssaV Salmonella* and treated with MG132. Cells
610 were analysed by flow cytometry and amounts of surface mMHCII in HA-positive cells are expressed
611 as a percentage of HA-negative cells in the same sample. Mean of three independent experiments
612 done in duplicate ± SD. Data were analysed by one-way ANOVA followed by Dunnett's multiple
613 comparison test, ** $p<0.01$, n.s. – not significant.

614 (C) Protein immunoblots of membrane fractionation samples from Mel Juso cells infected with *ΔsteD*
615 *Salmonella* strains carrying a plasmid expressing SteD-HA (wt or mutants) and treated with MG132.
616 Samples were taken from the pellet (P) and supernatant (S) of the total sample, after urea wash and
617 after RIPA wash.

618 (D) Representative confocal immunofluorescence microscopy images of Mel Juso cells infected with
619 *ΔsteD Salmonella* strains carrying a plasmid expressing SteD-HA (wt or mutants) and treated with
620 MG132. Cells were fixed and processed for immunofluorescence microscopy by labelling for HA
621 (green), the TGN (TGN46, red), and DNA (DAPI, blue). Arrowheads indicate cellular aggregates. Scale
622 bar – 10 µm.

623 (E) Quantification of HA signal at the TGN of cells represented in Fig 3D. The fluorescence intensity of
624 the HA signal at the TGN was measured in relation to total cellular fluorescence. Data are
625 representative of three independent experiments. Each dot represents the value for one cell. Mean ±
626 SD. The $\log_{10}$ fold change of the data were analysed by one-way ANOVA followed by Dunnett's
627 multiple comparison test, *** $p<0.001$.

628 Fig 4 – SteD integrates into membranes of the early secretory pathway

629 (A) Representative confocal immunofluorescence microscopy images of Mel JuSo cells expressing
630 GFP-SteD (wt or mutant) under a doxycycline-regulated promoter and the ER marker mCherry-ER-3.
631 Cells were either treated with doxycycline plus MG132 (dox) or treated with BFA followed by
632 doxycycline, MG132 and BFA (BFA-dox). Cells were then fixed and processed for immunofluorescence
633 microscopy by labelling for the TGN (TGN46, grey), and DNA (DAPI, blue). Scale bar – 10 µm.

634 (B) Quantification of cells represented in Fig 4A. Pearson's correlation coefficients for colocalization
635 between GFP-SteD and mCherry-ER-3 or TGN46. Data are representative of three independent
636 experiments. Each dot represents the value for one cell. Mean ± SD. Data were analysed by paired t-
637 test *** $p<0.001$, ** $p<0.01$.

638 (C) Protein immunoblots of membrane fractionation samples from Mel Juso cells expressing GFP-SteD
639 under a doxycycline-regulated promoter and treated as in Fig 4A. Samples were taken from the pellet
640 (P) and supernatant (S) of the total sample, after urea wash and after RIPA wash.

641 (D) mMHCII surface levels of Mel JuSo cells expressing GFP-SteD under a doxycycline-regulated
642 promoter or GFP and treated as in Fig 4A. Cells were analysed by flow cytometry and amounts of
643 surface mMHCII in GFP-positive cells are expressed as a percentage of GFP-negative cells in the same

644 sample. Mean of three independent experiments done in duplicate ± SD. Data were analysed by one-
645 way ANOVA followed by Dunnett's multiple comparison test, ** p<0.01, n.s. – not significant.

646 Fig 5 – AP1 mediates post-TGN trafficking of SteD

647 (A) Protein immunoblots of whole-cell lysates (Input) and immunoprecipitation with GFP-trap beads
648 (GFP IP) from Mel Juso cells expressing GFP-SteD or GFP-SseG following crosslinking with DSP. AP1 –
649 antibody specific for the γ subunit, AP2 – antibody specific for the α subunit, AP3 – antibody specific
650 for the δ subunit.

651 (B) Levels of immunoprecipitated AP1 were calculated by densitometry from immunoblots as
652 represented in Fig 5A. Protein levels were normalised to GFP-SteD. Mean of three independent
653 experiments ± SD. The data were analysed by one sample t-test, ** p<0.01.

654 (C) Protein immunoblots of Mel JuSo cells treated with scrambled siRNA (SCR) or siRNA specific to the
655 β subunit of AP1, the μ subunit of AP2 or the δ subunit of AP3. AP1 – antibody specific for the β
656 subunit, AP2 – antibody specific for the α subunit AP3 – antibody specific for the δ subunit.

657 (D) Representative confocal immunofluorescence microscopy images of Mel JuSo cells expressing
658 GFP-SteD after treatment with scrambled siRNA (SCR) or siRNA specific to the β subunit of AP1. Cells
659 were fixed and processed for immunofluorescence microscopy by labelling for MHCII compartments
660 (mMHCII, red), and DNA (DAPI, blue). Arrowheads indicate MHCII compartments. Scale bar – 10 μm.

661 (E) Mander's overlap coefficient of the fraction of GFP-SteD positive pixels that colocalise with
662 mMHCII positive pixels from cells after treatment with siRNA as in Fig 5C and D. Data are
663 representative of three independent experiments. Each dot represents the value for one cell. Mean ±
664 SD. Data were analysed by one-way ANOVA followed by Dunnett's multiple comparison test, ***
665 p<0.001, n.s. – not significant.

666 Fig 6 – The N-terminal tail of SteD is required for trafficking to MHCII
667 compartments

668 (A) Schematics of SteD showing predicted transmembrane domains and extent of truncation
669 mutations as indicated.

670 (B) Protein immunoblots of membrane fractionation samples from Mel Juso cells expressing GFP-SteD
671 (wt or mutants). Samples were taken from the pellet (P) and supernatant (S) of the total sample, after
672 urea wash and after RIPA wash.

673 (C) Representative confocal immunofluorescence microscopy images of Mel JuSo cells expressing
674 GFP-SteD (wt or mutants). Cells were fixed and processed for immunofluorescence microscopy by
675 labelling for MHCII compartments (mMHCII, red), the TGN (TGN46, grey), and DNA (DAPI, blue).
676 Arrowheads indicate MHCII compartments. Scale bar – 10 μm.

677 (D) Quantification of GFP at the surface of cells represented in Fig 6C. The fluorescence intensity of
678 the GFP signal at the surface of cells was measured in relation to total cellular fluorescence. Data are
679 representative of three independent experiments. Each dot represents the value for one cell. Mean ±
680 SD. The $\log_{10}$ fold change of the data were analysed by one-way ANOVA followed by Dunnett's
681 multiple comparison test, *** p<0.001, n.s. – not significant.

682 ## Fig 7 – A dileucine motif-like sequence in the N-terminal tail of SteD mediates
683 post-TGN trafficking

684 (A) Amino acid sequence of SteD showing predicted transmembrane domains. The N- and C-terminal
685 residues are highlighted in blue and red respectively. The residues substituted to alanines in
686 $SteD_{F32A,Y35A}$ and $SteD_{L13A,L14A,E18A,R19A}$ are highlighted in grey and green respectively.

687 (B) Representative confocal immunofluorescence microscopy images of Mel Juso cells infected with
688 *ΔsteD Salmonella* strains carrying a plasmid expressing SteD-HA (wt or mutant). Cells were fixed and
689 processed for immunofluorescence microscopy by labelling for HA (green), MHCII compartments
690 (mMHCII, red), and DNA (DAPI, blue). Arrowheads indicate MHCII compartments. Scale bar – 10 µm.

691 (C) Quantification of HA signal at the surface of cells represented in Fig 7B. The fluorescence intensity
692 of the HA signal at the cell surface was measured in relation to total cellular fluorescence. Data are
693 representative of three independent experiments. Each dot represents the value for one cell. Mean ±
694 SD. The $\log_{10}$ fold change of the data were analysed by t-test, *** $p<0.001$.

695 (D) Mander's overlap coefficient of the fraction of SteD-HA positive pixels that colocalise with mMHCII
696 positive pixels from cells as represented in Fig 7B. Data are representative of three independent
697 experiments. Each dot represents the value for one cell. Mean ± SD. Data were analysed by t-test, ***
698 $p<0.001$.

699 (E) mMHCII surface of Mel Juso cells infected with *ΔsteD Salmonella* carrying a plasmid expressing
700 SteD-HA (wt or mutant). Cells were analysed by flow cytometry and amounts of surface mMHCII in
701 infected cells are expressed as a percentage of uninfected cells in the same sample. Mean of three
702 independent experiments done in duplicate ± SD. Data were analysed by paired t-test, * $p<0.05$.

703 (F) Protein immunoblots of whole-cell lysates (Input) and immunoprecipitation with HA beads (HA IP)
704 from Mel Juso cells infected with *ΔsteD Salmonella* strains carrying a plasmid expressing SteD-HA (wt
705 or mutant) or SseF-HA following crosslinking with DSP. Mutation of charged residues might explain the
706 difference in migration through the SDS gel. AP1 – antibody specific for the γ subunit, AP2 – antibody
707 specific for the α subunit, AP3 – antibody specific for the δ subunit.

708 (G) Levels of immunoprecipitated AP1 were calculated by densitometry from immunoblots as
709 represented in Fig 7F. Protein levels were normalised to wt SteD-HA. Mean of three independent
710 experiments ± SD. The data were analysed by one sample t-test, *** $p<0.001$, n.s. – not significant.

711 ## Fig 8 – Model of SteD membrane integration and localisation

712 Following translocation from Salmonella (green) into the cytoplasm SteD (orange) is recruited to the
713 membranes of the early secretory pathway where it integrates. SteD then migrates to and
714 accumulates within the TGN. Through interaction with the AP1 complex (pink) it is trafficked to MHCII
715 compartments, where it interacts with mMHCII (dark green), which is ubiquitinated through the
716 actions of TMEM127 (brown) and WWP2 (red) causing a reduction in mMHCII surface levels.

717 $SteD_{L42A,M43A}$ mutation prevents membrane recruitment leading to aggregation in the cytoplasm.
718 $SteD_{S68A,G69A}$ mutation prevents membrane integration resulting in a Golgi-associated non-integrative
719 state. $SteD_{L13A,L14A,E18A,R19A}$ mutation prevents AP1 interaction leading to mis-trafficking of SteD to the
720 plasma membrane.

Supporting Information

Fig S1

(A) Amino acid sequence of SteD showing regions of amino acids substituted to alanine in alanine scanning mutagenesis.

(B) Representative flow cytometry plots showing the gating strategy for GFP-positive cells and negative cells as used for Fig 1C.

(C) mMHCII surface levels of Mel JuSo cells expressing GFP or GFP-SteD and treated with DMSO or MG132 were measured by flow cytometry. Mean of three independent experiments done in duplicate ± SD. Data were analysed by paired t-test, ** $p<0.01$, n.s. – not significant.

Fig S2

(A) Representative confocal immunofluorescence microscopy images of Mel JuSo cells expressing GFP-SteD (wt or mutants) after MG132 treatment. Cells were fixed and processed for immunofluorescence microscopy by labelling for ubiquitin (UB, red), and DNA (DAPI, blue). Arrowheads indicate cellular aggregates. Scale bar – 10 µm.

Fig S3

(A and D) Protein immunoblots of whole-cell lysates (WCL) and post-nuclear supernatant (PNS) of Mel Juso cells infected with *ΔsteD Salmonella* strains carrying a plasmid expressing SteD-HA (wt or mutants) and treated with MG132 or DMSO carrier. Actin and DnaK represent host cell and *Salmonella* loading controls respectively.

(B and C) mMHCII surface levels of Mel JuSo cells expressing GFP or GFP-SteD (wt or mutants) and treated with MG132. Cells were analysed by flow cytometry and amounts of surface mMHCII in GFP-positive cells are expressed as a percentage of GFP-negative cells in the same sample. Mean of three independent experiments done in duplicate ± SD. Data were analysed by one-way ANOVA followed by Dunnett's multiple comparison test in comparison to wt SteD, *** $p<0.001$, ** $p<0.01$, * $p<0.05$, n.s. – not significant.

(E) Representative flow cytometry plots showing the gating strategy for HA-positive and negative cells as used for Fig 3B.

Fig S4

(A) Representative confocal immunofluorescence microscopy images of Mel JuSo cells expressing GFP-SteD under a doxycycline-regulated promoter. Cells were either treated with doxycycline for 4 h (dox) or treated with BFA for 3 h followed by doxycycline and BFA for 4 h (BFA-dox). Cells were then fixed and processed for immunofluorescence microscopy by labelling for MHCII compartments (mMHCII, red), the TGN (TGN46, grey), and DNA (DAPI, blue). Arrowheads indicate MHCII compartments. Scale bar – 10 µm.

(B) Representative flow cytometry plots showing the gating strategy for GFP-positive and negative cells as used for Fig 4D.

757 (C) Confocal microscopy images demonstrating photobleaching of a Mel JuSo cell expressing GFP-
758 SteD from Video S2. Closed arrowheads indicate anterograde vesicle traffic from the Golgi region.
759 Barbed arrowhead indicates retrograde vesicle traffic. Scale bar – 10 µm.

760 ## Fig S5

761 (A) mMHCII surface levels of Mel JuSo cells expressing GFP-SteD and treated with scrambled siRNA
762 (SCR) or siRNA specific to the β subunit of AP1. Cells were analysed by flow cytometry and amounts of
763 surface mMHCII in GFP-positive cells are expressed as a percentage of GFP-negative cells in the same
764 sample. Mean of three independent experiments done in duplicate ± SD. Data were analysed by one-
765 way ANOVA followed by Dunnett's multiple comparison test n.s. – not significant.

766 (B) Quantification of GFP at the surface of cells represented in Fig 5D. The fluorescence intensity of
767 the GFP signal at the surface of cells was measured in relation to total cellular fluorescence. Data are
768 representative of three independent experiments. Each dot represents the value for one cell. Mean ±
769 SD. The $\log_{10}$ fold change of the data were analysed by t-test, n.s. – not significant.

770 ## Fig S6

771 (A) Protein immunoblots of Mel JuSo cells expressing GFP or GFP-SteD (wt or mutants).

772 (B) Quantification of GFP at the TGN of cells represented in Fig 6C. The fluorescence intensity of the
773 GFP signal at the TGN was measured in relation to total cellular fluorescence. Data are representative
774 of three independent experiments. Each dot represents the value for one cell. Mean ± SD. The $\log_{10}$
775 fold change of the data were analysed by one-way ANOVA followed by Dunnett's multiple comparison
776 test, *** $p<0.001$, n.s. – not significant.

777 (C) Confocal microscopy images demonstrating photoactivation of a Mel JuSo cell expressing mEos-
778 SteD (wt or 37-111) from Video S3. Red dotted circles indicate photo-activated areas. Red arrowheads
779 indicate Golgi-derived vesicles. Scale bar – 10 µm.

780 ## Fig S7

781 (A) mMHCII surface levels of Mel JuSo cells expressing GFP or GFP-SteD (wt or mutants). Cells were
782 analysed by flow cytometry and amounts of surface mMHCII in GFP-positive cells are expressed as a
783 percentage of GFP negative cells in the same sample. Mean of three independent experiments done
784 in duplicate ± SD. Data were analysed by one-way ANOVA followed by Dunnett's multiple comparison
785 test compared to wt SteD, *** $p<0.001$, ** $p<0.01$, n.s. – not significant.

786 (B) mMHCII surface of Mel Juso cells infected with *ΔsteD Salmonella* carrying a plasmid expressing SteD-
787 HA (wt or mutant). Cells were analysed by flow cytometry and amounts of surface mMHCII in infected
788 cells are expressed as a percentage of uninfected cells in the same sample. Mean of three independent
789 experiments done in duplicate ± SD. Data were analysed by one-way ANOVA followed by Dunnett's
790 multiple comparison test, *** $p<0.001$, n.s. – not significant.

791 (C) Representative confocal immunofluorescence microscopy images of Mel JuSo cells expressing
792 GFP-SteD (wt or mutants). Cells were fixed and processed for immunofluorescence microscopy by
793 labelling for MHCII compartments (mMHCII, red), the TGN (TGN46, grey), and DNA (DAPI, blue).
794 Arrowheads indicate MHCII compartments. Scale bar – 10 µm.

795 (D) Quantification of GFP at the surface of cells represented in Fig S7C. The fluorescence intensity of
796 the GFP signal at the cell surface was measured in relation to total cellular fluorescence. Data are
797 representative of three independent experiments. Each dot represents the value for one cell. Mean ±
798 SD. The $\log_{10}$ fold change of the data were analysed by one-way ANOVA followed by Dunnett's
799 multiple comparison test, *** $p<0.001$, n.s. – not significant.

800 (E) Mander's overlap coefficient of the fraction of GFP-SteD positive pixels that colocalise with
801 mMHCII positive pixels from cells as represented in Fig S7C. Data are representative of three
802 independent experiments. Each dot represents the value for one cell. Mean ± SD. Data were analysed
803 by one-way ANOVA followed by Dunnett's multiple comparison test, *** $p<0.001$, n.s. – not
804 significant.

805 (F) Protein immunoblots of whole-cell lysates (Input) and immunoprecipitation with GFP-trap beads
806 (GFP IP) from Mel Juso cells expressing GFP-SteD (wt or mutants) or GFP-SseG following crosslinking
807 with DSP. Mutation of charged residues might explain the difference in migration through the SDS gel.
808 AP1 – antibody specific for the γ subunit, AP2 – antibody specific for the α subunit, AP3 – antibody
809 specific for the δ subunit.

810 (G) Levels of immunoprecipitated AP1 and TMEM127 were calculated by densitometry from
811 immunoblots as represented in Fig S7F. Protein levels were normalised to GFP-SteD. Mean of three
812 independent experiments ± SD. The data were analysed by one sample t-test, *** $p<0.001$, * $p<0.05$,
813 n.s. – not significant.

814 (H) Representative confocal immunofluorescence microscopy images of Mel Juso cells infected with
815 *ΔsteD Salmonella* strains carrying a plasmid expressing SteD-HA (wt or mutant). Cells were fixed and
816 processed for immunofluorescence microscopy by labelling for HA (green), the TGN (TGN46, red), and
817 DNA (DAPI, blue). Scale bar – 10 µm.

818 Video S1

819 Time-lapse microscopy of Mel JuSo cells expressing GFP-SteD (wt or mutant) treated with MG132.
820 Scale bar – 10 µm.

821 Video S2

822 Time-lapse microscopy of Mel JuSo cells expressing GFP-SteD following photobleaching of non-Golgi
823 regions. Scale bar – 10 µm.

824 Video S3

825 Time-lapse microscopy of Mel JuSo cells expressing mEos-SteD (wt or mutant) following activation of
826 mEos in Golgi regions. Scale bar – 10 µm.

827 Table S1 – *S.* Typhimurium strains used in this study

828 Table S2 – Plasmids used in this study

829 Table S3 – Primary antibodies used in this study

Fig 1

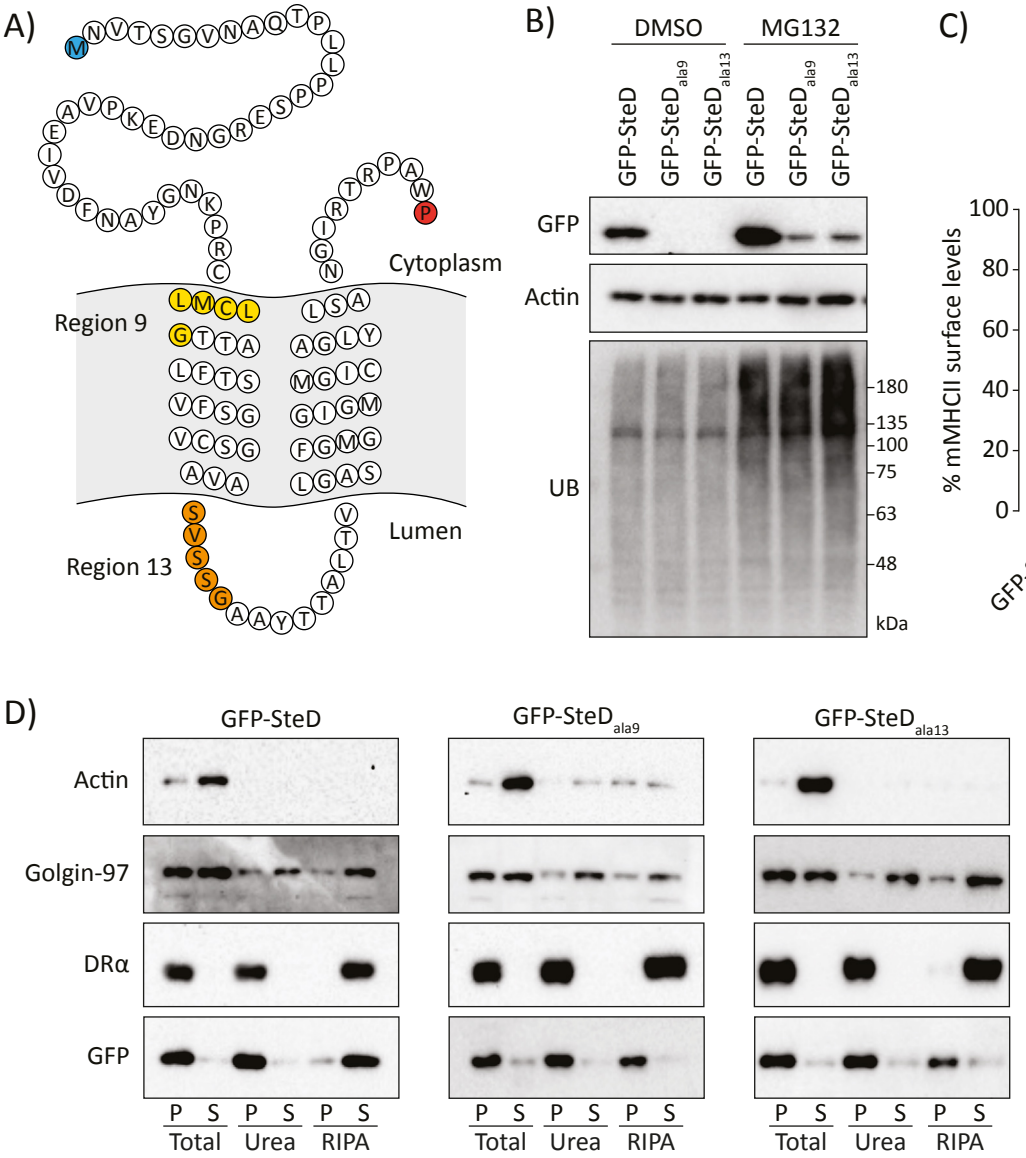

Fig 1 – Two regions of SteD are required for membrane integration

(A) Amino acid sequence of SteD showing predicted transmembrane domains. The N- and C-terminal residues are highlighted in blue and red respectively. The residues substituted to alanines in $SteD_{ala9}$ and $SteD_{ala13}$ mutants are highlighted in yellow and orange respectively.

(B) Protein immunoblots of whole-cell lysates derived from Mel JuSo cells expressing GFP-SteD (wt or mutants) and treated with MG132 or DMSO carrier. UB – ubiquitin.

(C) mMHCII surface levels of Mel JuSo cells expressing GFP or GFP-SteD (wt or mutants) and treated with MG132. Cells were analysed by flow cytometry and amounts of surface mMHCII in GFP-positive cells are expressed as a percentage of GFP-negative cells in the same sample. Mean of three independent experiments done in duplicate ± SD. Data were analysed by one-way ANOVA followed by Dunnett's multiple comparison test, *** $p<0.001$, n.s. – not significant.

(D) Protein immunoblots of membrane fractionation samples from Mel Juso cells expressing GFP-SteD (wt or mutants) and treated with MG132. Samples were taken from the pellet (P) and supernatant (S) of the total sample, after urea wash and after RIPA wash.

Fig 2

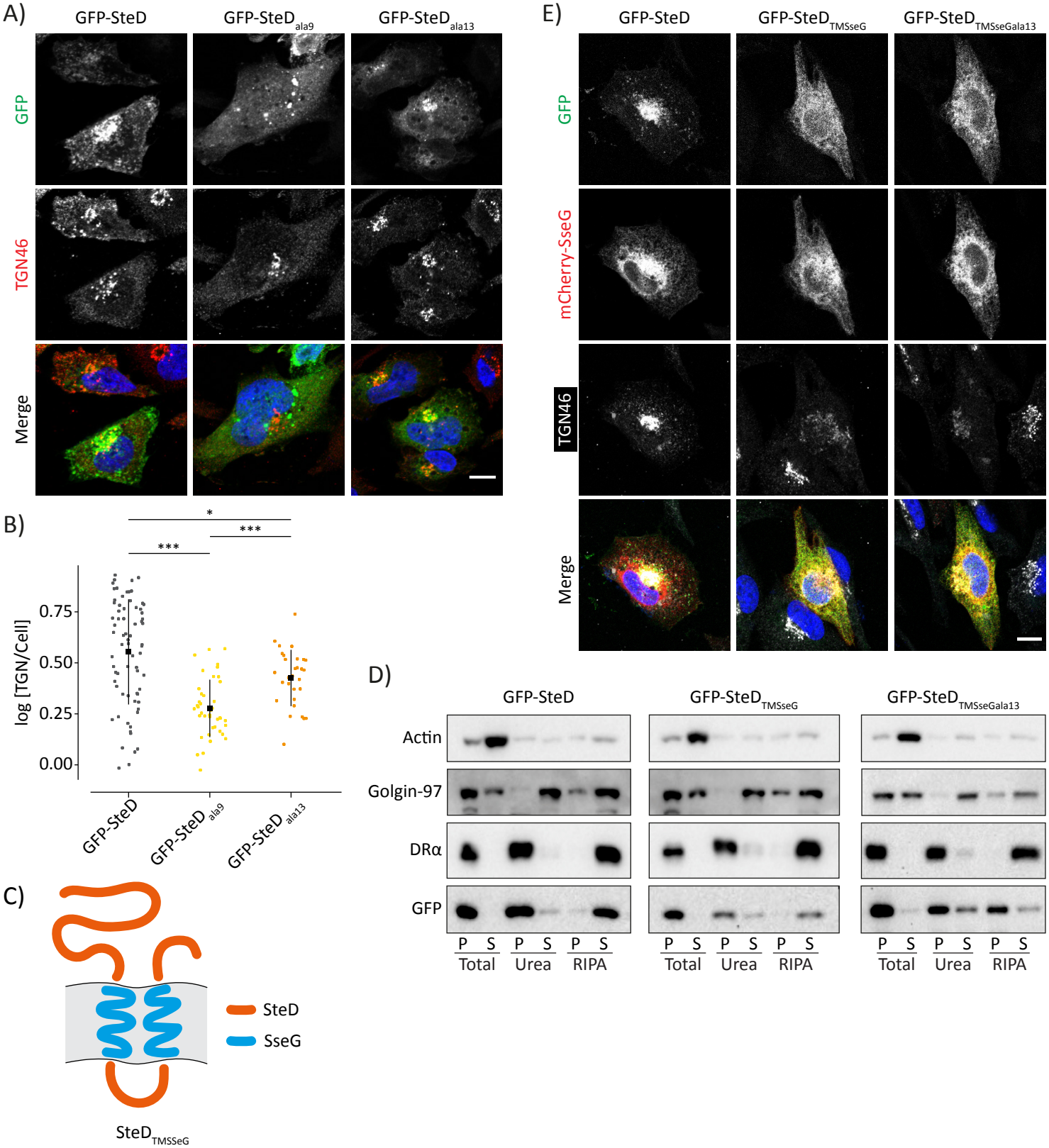

Fig 2 – Recruitment of SteD to the TGN is independent from membrane integration

(A) Representative confocal immunofluorescence microscopy images of Mel JuSo cells expressing GFP-SteD (wt or mutants) after MG132 treatment. Cells were fixed and processed for immunofluorescence microscopy by labelling for the TGN (TGN46, red), and DNA (DAPI, blue). Scale bar – 10 µm.

(B) Quantification of GFP at the TGN of cells represented in Fig 2A. The fluorescence intensity of the GFP signal at the TGN was measured in relation to total cellular fluorescence. Data are representative of three independent experiments. Each dot represents the value for one cell. Mean ± SD. The $\log_{10}$ fold change of the data were analysed by one-way ANOVA followed by Dunnett's multiple comparison test, *** $p<0.001$, * $p<0.05$.

(C) Schematic of SteD chimera with transmembrane domains of SseG.

(D) Protein immunoblots of membrane fractionation samples from Mel Juso cells expressing GFP-SteD (wt or chimeric mutants) and treated with MG132. Samples were taken from the pellet (P) and supernatant (S) of the total sample, after urea wash and after RIPA wash.

(E) Representative confocal immunofluorescence microscopy images of Mel JuSo cells expressing GFP-SteD (wt or chimeric mutants) and mCherry-SseG after MG132 treatment. Cells were fixed and processed for immunofluorescence microscopy by labelling for the TGN (TGN46, grey), and DNA (DAPI, blue). Scale bar – 10 µm.

Fig 3

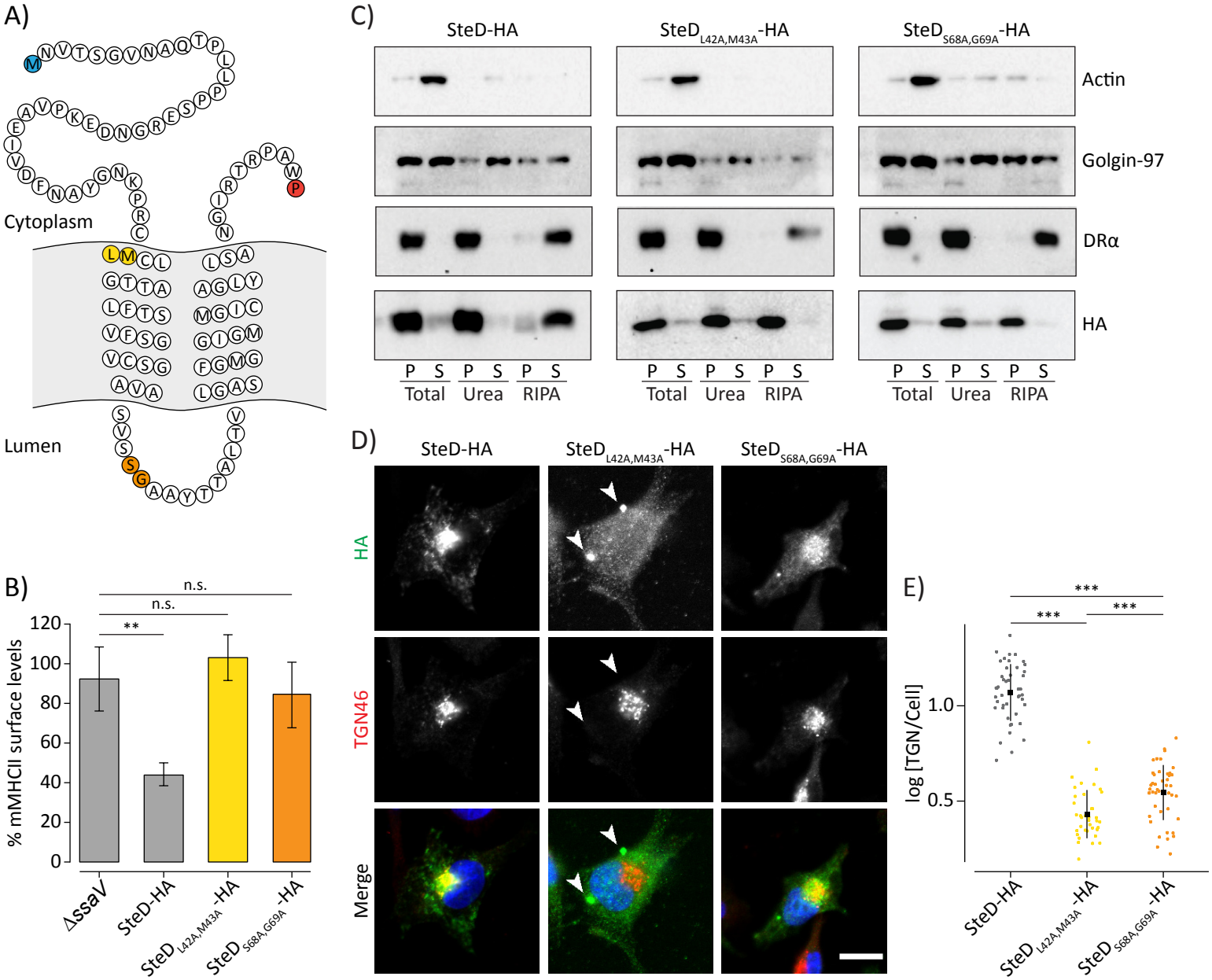

Fig 3 – Membrane integration following translocation

(A) Amino acid sequence of SteD showing predicted transmembrane domains. The N- and C-terminal residues are highlighted in blue and red respectively. The residues substituted to alanines in $SteD_{L42A,M43A}$ and $SteD_{S68A,G69A}$ mutants are highlighted in yellow and orange respectively.

(B) mMHCII surface levels of Mel JuSo cells infected with *ΔsteD Salmonella* carrying a plasmid expressing SteD-HA (wt or mutants) or SPI-2 null *ΔssaV Salmonella* and treated with MG132. Cells were analysed by flow cytometry and amounts of surface mMHCII in HA-positive cells are expressed as a percentage of HA-negative cells in the same sample. Mean of three independent experiments done in duplicate ± SD. Data were analysed by one-way ANOVA followed by Dunnett's multiple comparison test, ** $p<0.01$, n.s. – not significant.

(C) Protein immunoblots of membrane fractionation samples from Mel Juso cells infected with *ΔsteD Salmonella* strains carrying a plasmid expressing SteD-HA (wt or mutants) and treated with MG132. Samples were taken from the pellet (P) and supernatant (S) of the total sample, after urea wash and after RIPA wash.

(D) Representative confocal immunofluorescence microscopy images of Mel Juso cells infected with *ΔsteD Salmonella* strains carrying a plasmid expressing SteD-HA (wt or mutants) and treated with MG132. Cells were fixed and processed for immunofluorescence microscopy by labelling for HA (green), the TGN (TGN46, red), and DNA (DAPI, blue). Arrowheads indicate cellular aggregates. Scale bar – 10 µm.

(E) Quantification of HA signal at the TGN of cells represented in Fig 3D. The fluorescence intensity of the HA signal at the TGN was measured in relation to total cellular fluorescence. Data are representative of three independent experiments. Each dot represents the value for one cell. Mean ± SD. The log_{10} fold change of the data were analysed by one-way ANOVA followed by Dunnett's multiple comparison test, *** $p<0.001$.

Fig 4

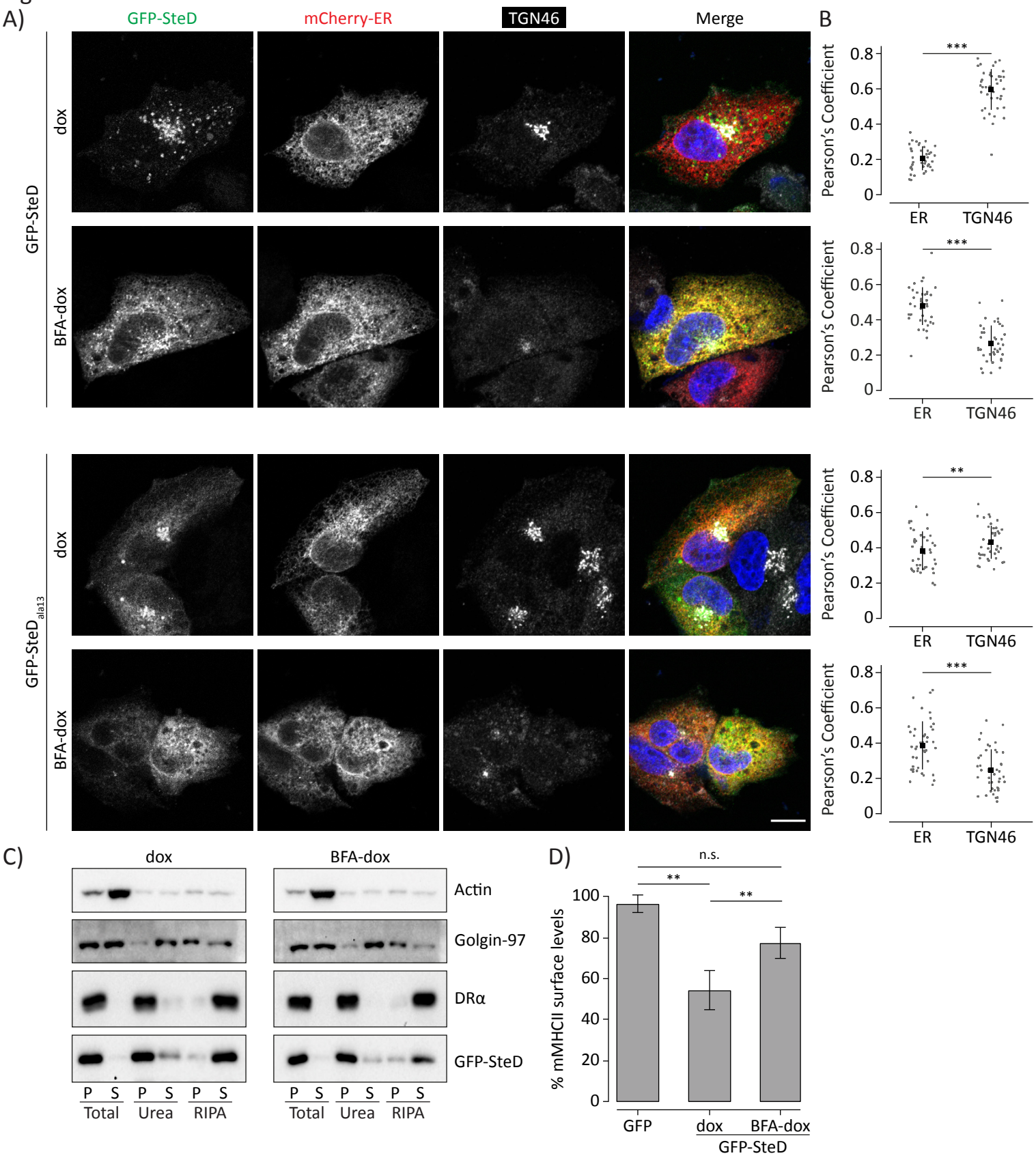

Fig 4 – SteD integrates into membranes of the early secretory pathway

(A) Representative confocal immunofluorescence microscopy images of Mel JuSo cells expressing GFP-SteD (wt or mutant) under a doxycycline-regulated promoter and the ER marker mCherry-ER-3. Cells were either treated with doxycycline plus MG132 (dox) or treated with BFA followed by doxycycline, MG132 and BFA (BFA-dox). Cells were then fixed and processed for immunofluorescence microscopy by labelling for the TGN (TGN46, grey), and DNA (DAPI, blue). Scale bar – 10 µm.

(B) Quantification of cells represented in Fig 4A. Pearson's correlation coefficients for colocalization between GFP-SteD and mCherry-ER-3 or TGN46. Data are representative of three independent experiments. Each dot represents the value for one cell. Mean ± SD. Data were analysed by paired t-test *** $p<0.001$, ** $p<0.01$.

(C) Protein immunoblots of membrane fractionation samples from Mel Juso cells expressing GFP-SteD under a doxycycline-regulated promoter and treated as in Fig 4A. Samples were taken from the pellet (P) and supernatant (S) of the total sample, after urea wash and after RIPA wash.

(D) mMHCII surface levels of Mel JuSo cells expressing GFP-SteD under a doxycycline-regulated promoter or GFP and treated as in Fig 4A. Cells were analysed by flow cytometry and amounts of surface mMHCII in GFP-positive cells are expressed as a percentage of GFP-negative cells in the same sample. Mean of three independent experiments done in duplicate ± SD. Data were analysed by one-way ANOVA followed by Dunnett's multiple comparison test, ** $p<0.01$, n.s. – not significant.

Fig 5

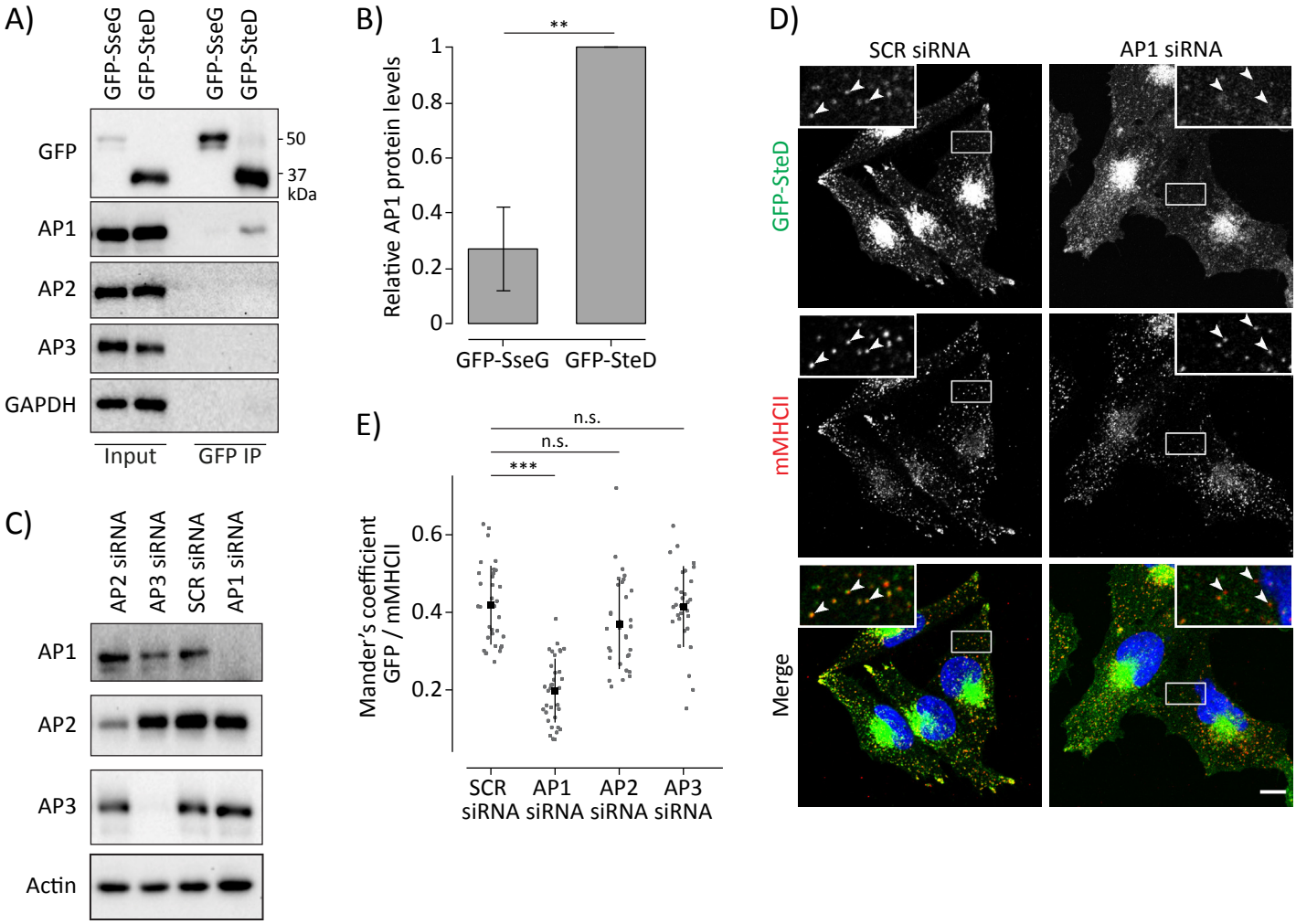

Fig 5 – AP1 mediates post-TGN trafficking of SteD

(A) Protein immunoblots of whole-cell lysates (Input) and immunoprecipitation with GFP-trap beads (GFP IP) from Mel Juso cells expressing GFP-SteD or GFP-SseG following crosslinking with DSP. AP1 – antibody specific for the γ subunit, AP2 – antibody specific for the α subunit, AP3 – antibody specific for the δ subunit.

(B) Levels of immunoprecipitated AP1 were calculated by densitometry from immunoblots as represented in Fig 5A. Protein levels were normalised to GFP-SteD. Mean of three independent experiments ± SD. The data were analysed by one sample t-test, ** $p<0.01$.

(C) Protein immunoblots of Mel JuSo cells treated with scrambled siRNA (SCR) or siRNA specific to the β subunit of AP1, the μ subunit of AP2 or the δ subunit of AP3. AP1 – antibody specific for the β subunit, AP2 – antibody specific for the α subunit AP3 – antibody specific for the δ subunit.

(D) Representative confocal immunofluorescence microscopy images of Mel JuSo cells expressing GFP-SteD after treatment with scrambled siRNA (SCR) or siRNA specific to the β subunit of AP1. Cells were fixed and processed for immunofluorescence microscopy by labelling for MHCII compartments (mMHCII, red), and DNA (DAPI, blue). Arrowheads indicate MHCII compartments. Scale bar – 10 μm.

(E) Mander's overlap coefficient of the fraction of GFP-SteD positive pixels that colocalise with mMHCII positive pixels from cells after treatment with siRNA as in Fig 5C and D. Data are representative of three independent experiments. Each dot represents the value for one cell. Mean ± SD. Data were analysed by one-way ANOVA followed by Dunnett's multiple comparison test, *** $p<0.001$, n.s. – not significant.

Fig 6

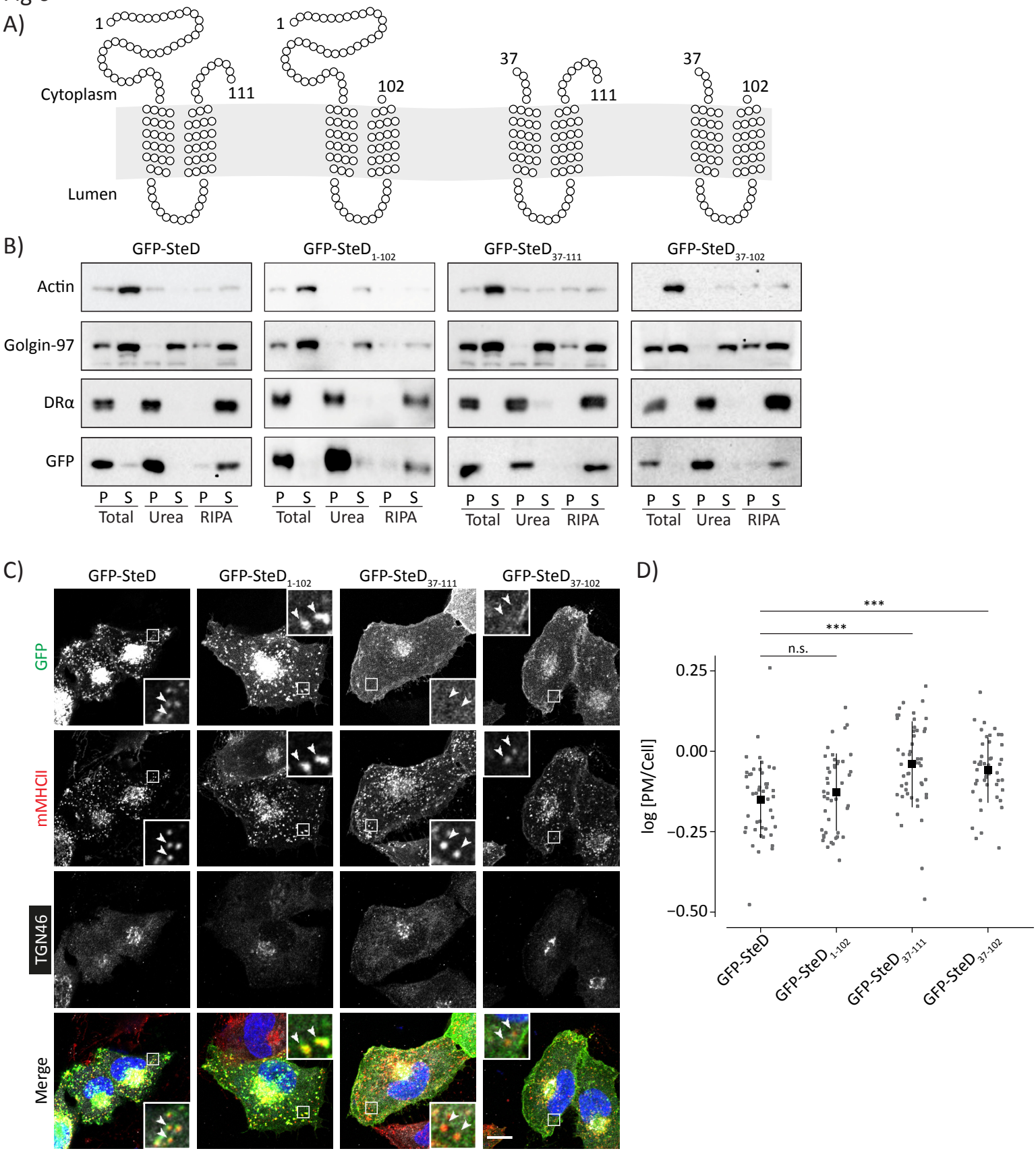

Fig 6 – The N-terminal tail of SteD is required for trafficking to MHCII compartments

(A) Schematics of SteD showing predicted transmembrane domains and extent of truncation mutations as indicated.

(B) Protein immunoblots of membrane fractionation samples from Mel Juso cells expressing GFP-SteD (wt or mutants). Samples were taken from the pellet (P) and supernatant (S) of the total sample, after urea wash and after RIPA wash.

(C) Representative confocal immunofluorescence microscopy images of Mel JuSo cells expressing GFP-SteD (wt or mutants). Cells were fixed and processed for immunofluorescence microscopy by labelling for MHCII compartments (mMHCII, red), the TGN (TGN46, grey), and DNA (DAPI, blue). Arrowheads indicate MHCII compartments. Scale bar – 10 µm.

(D) Quantification of GFP at the surface of cells represented in Fig 6C. The fluorescence intensity of the GFP signal at the surface of cells was measured in relation to total cellular fluorescence. Data are representative of three independent experiments. Each dot represents the value for one cell. Mean ± SD. The $\log_{10}$ fold change of the data were analysed by one-way ANOVA followed by Dunnett's multiple comparison test, *** $p<0.001$, n.s. – not significant.

Fig 7

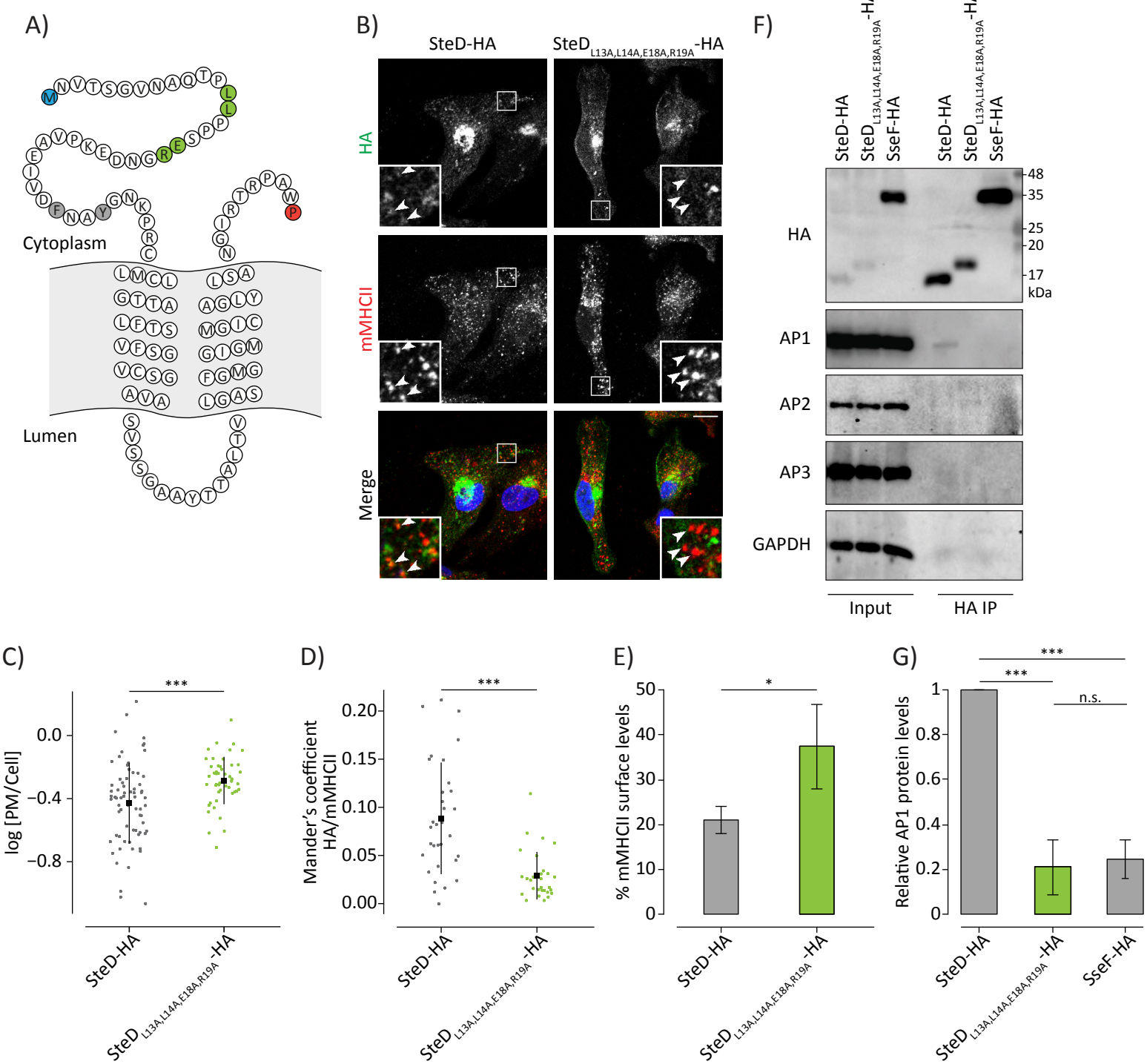

Fig 7 – A dileucine motif-like sequence in the N-terminal tail of SteD mediates post-TGN trafficking

(A) Amino acid sequence of SteD showing predicted transmembrane domains. The N- and C-terminal residues are highlighted in blue and red respectively. The residues substituted to alanines in $SteD_{F32A,Y35A}$ and $SteD_{L13A,L14A,E18A,R19A}$ are highlighted in grey and green respectively.

(B) Representative confocal immunofluorescence microscopy images of Mel Juso cells infected with *ΔsteD Salmonella* strains carrying a plasmid expressing SteD-HA (wt or mutant). Cells were fixed and processed for immunofluorescence microscopy by labelling for HA (green), MHCII compartments (mMHCII, red), and DNA (DAPI, blue). Arrowheads indicate MHCII compartments. Scale bar – 10 µm.

(C) Quantification of HA signal at the surface of cells represented in Fig 7B. The fluorescence intensity of the HA signal at the cell surface was measured in relation to total cellular fluorescence. Data are representative of three independent experiments. Each dot represents the value for one cell. Mean ± SD. The $\log_{10}$ fold change of the data were analysed by t-test, *** $p<0.001$.

(D) Mander's overlap coefficient of the fraction of SteD-HA positive pixels that colocalise with mMHCII positive pixels from cells as represented in Fig 7B. Data are representative of three independent experiments. Each dot represents the value for one cell. Mean ± SD. Data were analysed by t-test, *** $p<0.001$.

(E) mMHCII surface of Mel Juso cells infected with *ΔsteD Salmonella* carrying a plasmid expressing SteD-HA (wt or mutant). Cells were analysed by flow cytometry and amounts of surface mMHCII in infected cells are expressed as a percentage of uninfected cells in the same sample. Mean of three independent experiments done in duplicate ± SD. Data were analysed by paired t-test, * $p<0.05$.

(F) Protein immunoblots of whole-cell lysates (Input) and immunoprecipitation with HA beads (HA IP) from Mel Juso cells infected with *ΔsteD Salmonella* strains carrying a plasmid expressing SteD-HA (wt or mutant) or SseF-HA following crosslinking with DSP. Mutation of charged residues might explain the difference in migration through the SDS gel. AP1 – antibody specific for the γ subunit, AP2 – antibody specific for the α subunit, AP3 – antibody specific for the δ subunit.

(G) Levels of immunoprecipitated AP1 were calculated by densitometry from immunoblots as represented in Fig 7F. Protein levels were normalised to wt SteD-HA. Mean of three independent experiments ± SD. The data were analysed by one sample t-test, *** $p<0.001$, n.s. – not significant.

Fig 8

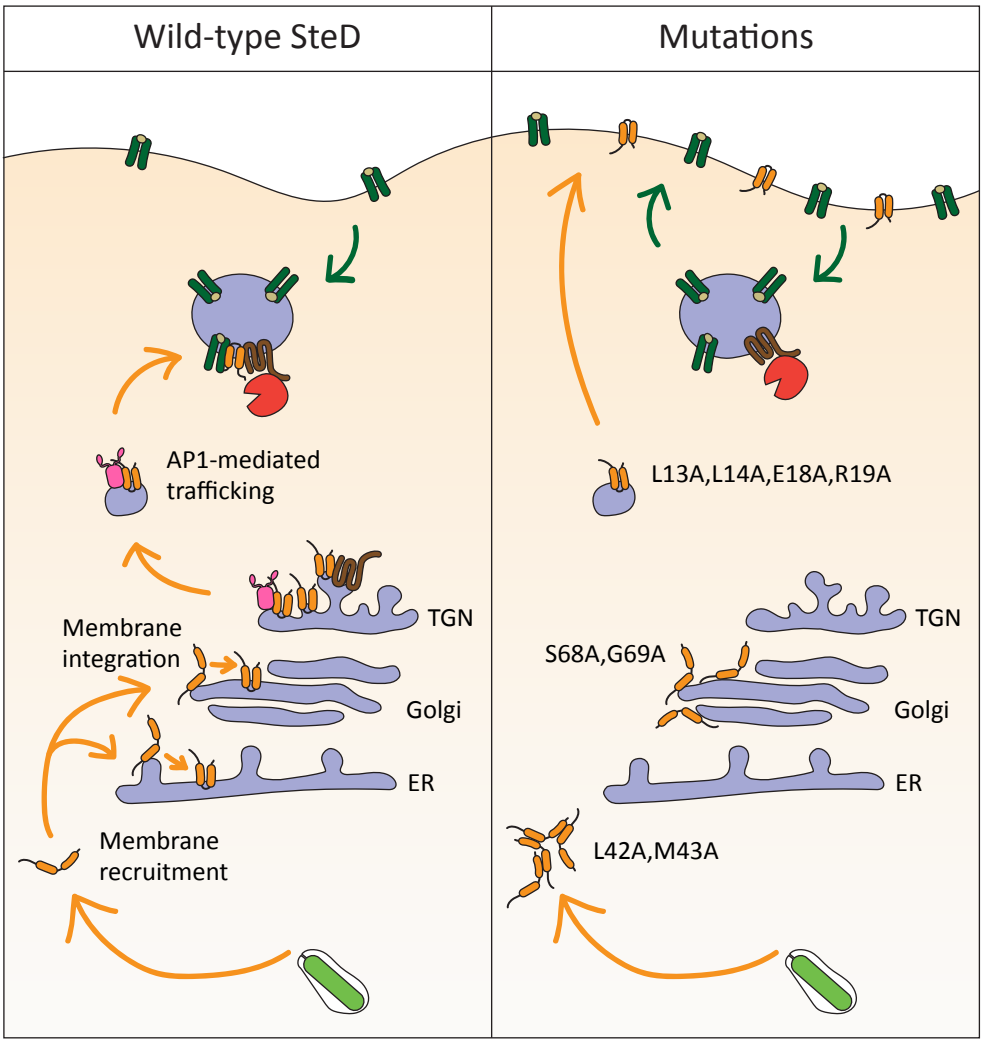

Fig 8 – Model of SteD membrane integration and localisation
Following translocation from *Salmonella* (green) into the cytoplasm SteD (orange) is recruited to the membranes of the early secretory pathway where it integrates. SteD then migrates to and accumulates within the TGN. Through interaction with the AP1 complex (pink) it is trafficked to MHCII compartments, where it interacts with mMHCII (dark green), which is ubiquitinated through the actions of TMEM127 (brown) and WWP2 (red) causing a reduction in mMHCII surface levels.

$SteD_{L42A,M43A}$ mutation prevents membrane recruitment leading to aggregation in the cytoplasm. $SteD_{S68A,G69A}$ mutation prevents membrane integration resulting in a Golgi-associated non-integrative state. $SteD_{L13A,L14A,E18A,R19A}$ mutation prevents AP1 interaction leading to mis-trafficking of SteD to the plasma membrane.